ORIGINAL ARTICLE

Perturbed State-Transition Matrix for Spacecraft Formation Flying Terminal-Point Guidance

Yazan Chihabi[1] (ORCID) **· Steve Ulrich[1]**

Abstract

This paper presents a guidance solution of relative motion between two spacecraft using relative classical orbital elements for on-board implementation purposes. The solution is obtained by propagating the relative orbital elements forward in time using a newly formulated state-transition matrix, while taking into account gravitational field up to the fifth harmonic, third-body effects up to the fourth order and drag, then calculating the relative motion in the local-vertical-local-horizontal reference frame at each time-step. Specifically, utilizing Jacobian matrices evaluated at the target spacecraft's initial orbital elements, the solution proposed in this paper requires only a single matrix multiplication with the initial orbital elements and the desired time to propagate relative orbital elements forward in time. The new solution is shown to accurately describe the relative motion when compared with a numerical simulator, yielding errors on the order of meters for separation distances on the order of thousands of meters. Additionally, the solution maintained accurate tracking performance when used within a back-propagation, or terminal-point, guidance law.

Keywords Spacecraft formation flying · Spacecraft relative motion · Spacecraft dynamics · Spacecraft formation flying guidance · Analytical · Orbital elements

Introduction

Formation flying of multiple spacecraft is a key technology for space-related ventures as it offers lower costs and increased efficiency by reducing the mass, power demand and size of the spacecraft buses when compared to the use of single spacecraft. For instance, NASA's MMS mission uses four spacecraft flying in formation in attempt to study the magnetosphere [36]. However, formation flying has many

---

✉ Yazan Chihabi
  yazanchihabi@cmail.carleton.ca

[1] 1125 Colonel By Drive, Ottawa, ON K1S 5B6, Canada

complexities when compared to that of single spacecraft missions. Fuel-efficient formation keeping and reconfiguration maneuvers require accurate guidance systems which calculates the required reference trajectory. Therefore, the guidance system must account for perturbations since ignoring orbital perturbations in the calculation of reference trajectories would result more propellant consumption than necessary. Formulations which take into account perturbations, such as the effects of gravitational field caused by oblateness of the earth, third body effects, and drag, can be found in literature. However, these formulations are only applied to single spacecraft. Furthermore, the dynamics model must be accurate for high eccentricity values, and large separation distances while remaining computationally in-expensive for onboard implementation purposes. Accurate numerical models which take into account perturbations exist; however, they are computationally expensive and can lead to errors due to integration tolerances. Therefore, an analytical dynamics model is required since it satisfies these conditions and does not require numerical integration.

The Hill-Clohessy-Wiltshire (HCW) model [3] provides linearized relative dynamics based upon exact Keplerian non-linear differential equations of motion in the LVLH (local-vertical-local-horizontal) reference frame. This model is assumes a circular Keplerian orbit and as a result, it is in-accurate for modeling elliptical reference orbits. Specifically, the errors increase with increasing eccentricity and not accounting for eccentricity in the HCW model can greatly outweigh the effects of external perturbations [16]. Gurfil and Kholshevnikov [12, 13] formulated an analytical nonlinear solution, first suggested by Hill [15], that incorporates Keplerian eccentric orbits and valid for any time-step. Taking advantage of classical orbital elements as constant parameters, the relative dynamics of a chaser spacecraft can be calculated (analogous to a simple rotation matrix approach) instead of using cartesian initial conditions in the HCW model. The most important advantage of using this approach is the fact that the orbital elements can be made to vary as a function of time to include the effects of orbital perturbations [11, 31]. Furthermore, Schaub [32, p. 593-673] extended Gurfil and Kholshevnikov's equations through linearizations such that the cartesian coordinates in the LVLH reference frame are expressed in terms of orbital element differences.

Recently, Kuiack and Ulrich [23] developed a novel method in propagating relative motion analytically. Specifically linearized short periodic and secular variations of the orbital elements formulated by Brouwer for the second zonal harmonic (J_2) [2] were implemented into Gurfil and Kholshevnikov's equations of motion [12, 13]. Using this formulation, Kuiack and Ulrich [23] implemented a back propagation technique such that a set of initial conditions for the chaser spacecraft in terms of orbital elements is found to allow the spacecraft to drift into a desired relative orbital elements. While the method presented in Kuiack and Ulrich [23] was highly accurate when modelling the effects of J_2, the solution does not account for other significant orbital perturbations and can only find Cartesian coordinates from relative orbital elements and not vice versa. The solution required the addition of periodic variations at every time-step to propagate the relative motion, while the solution presented here does not. Furthermore, the solution presented by [23] cannot be used in the development of highly sophisticated navigation and control algorithms since the

periodic variations are a function of mean orbital elements and cannot be expressed in state-space form.

A state-transition matrix (STM) for the perturbed relative motion that includes the first-order secular, long-period, and short-period effects due to the dominant second zonal harmonic perturbation was first proposed by Gim and Alfriend [8]. Specifically, the formulation utilized a linearized geometric method for mapping the osculating orbital element differences relative position and velocity in orbital frame. An analytical solution to propagate the averaged relative orbital elements about an oblate planet was proposed by Sengupta et al. [33]. Furthermore, Roscoe et al. [35] formulated a solution that included the effects of third-body perturbations on spacecraft relative motion. An analytical solution, proposed by Mahajan et al. [26], uses linearized state transition matrices to propagate the relative mean orbital elements forward in time while taking into account the effects of gravitational field perturbation up to an arbitrary degree and their respective long and short periodic effects. The development of this solution involves the use of Hamiltonians and is highly complex; however, once implemented, it is simple and accurate. The main advantage of this formulation is that it can be expanded to an arbitrary degree based on desired accuracy while taking into account the effects of tesseral harmonics. Additionally, Guffanti et al. [9] introduced a set of state transition matrices which included singly averaged effects of the second and third zonal harmonics, doubly-averaged third body expanded to the second order, and solar radiation pressure where non-singular orbital elements were used as the states. Further work was done by Guffanti et al. [19] in the development of STM formulations using singular, quasi singular and non-singular orbital elements that included the effects of J_2, second order expansion of the third-body disturbing function, and atmospheric drag effects on semi-major axis and eccentricity. Most literature addresses the problem of spacecraft relative motion in terms of obtaining an analytical solution that is accurate and analyzed for long term propagation and, in some cases, involves the use of mean to osculating conversions. Although the solutions are highly accurate, guidance and control applications require accurate dynamics for smaller time-scales and time-steps to be used with a continuous controller. In addition, the solutions required the target's perturbed orbital motion to be propagated forward in time to obtain the solution of relative motion.

In this context, the main contributions of this paper are: (1) a new way to obtain the linearized equations of relative motion on perturbed orbit using relative classical orbital elements and (2) a new perturbed state transition matrix formulation with application to a terminal-point guidance law. Unlike the one formulated by Guffanti, et al. [9] and Mahajan, et al. [26] the new STM formulation developed in this work includes the combined effects of gravitational, third-body and drag perturbations. Specifically, third body equations up to the fourth degree [6, 20, 22, 30], drag model by Lawden [24] and gravitational perturbation up to the fifth zonal harmonic [2, 21, 25] are utilized in the development of the new formulation. Lawden's atmospheric drag model allows to compute the variations in semi-major axis, eccentricity, inclination, argument of perigee and the right ascension of the ascending node. Additionally, the linearized equations developed by Schaub [32, p. 593-673] is used in the derivation of the STM relating relative orbital elements to relative position and velocity. By formulating a linear time invariant solution and including more perturbations, the

work presented in this paper aims to provide an simple and accurate solution to relative motion. However, one of the key differences when compared to the approach in [23] is the state-transition matrix approach and the determination of relative orbital elements using desired relative Cartesian coordinates instead of only using orbital elements.

This paper is organized as follows: "Linearized Equations of Relative Motion using Relative Orbital Elements" describes the linearized equations of motion formulated by Schaub [32, p. 593-673] and the proposed approach to derive STM to map relative relative orbital elements to Cartesian coordinates. "State Transition Matrix Formulation". provides the details of the derivation for the perturbed STM. Next, "Terminal-Point Guidance Law" provides a description of the newly developed terminal-point guidance law. "Numerical Simulations" presents simulation results for the developed solution and concluding remarks are provided in "Conclusion".

Linearized Equations of Relative Motion using Relative Orbital Elements

The non-linear equations of motion formulated by Gurfil and Kholshevnikov provides a method of calculating the relative motion of two spacecraft in the LVLH reference frame using each spacecraft's orbital elements [12, 13]. However, these equations cannot be used to determine relative orbital elements using a set of desired Cartesian coordinates. Therefore, a set of linearized equations that describe the relative motion must be used.

The LVLH reference frame is denoted by $\mathcal{F}_L$ and defined by its orthonormal unit vectors $[L_x, L_y, L_z]^T$ with its origin at the target spacecraft. The unit vector L_z points in the same direction as the orbit's angular momentum vector normal to the orbital plane. L_x points in the direction of the target's inertial position r_t and L_y completing the triad such that $L_y = L_z \times L_x$. Schaub derived the linearized equations of motion using a first order approximation and is presented in state-space form below [32, p. 593-673]

$$\rho = \begin{bmatrix} x & y & z \end{bmatrix}^T = A_1 \Delta x \tag{1}$$

such that $\rho = \rho^T \mathcal{F}_L$ and

$$x = \begin{bmatrix} a & e & i & \omega & \Omega & M \end{bmatrix}^T \tag{2}$$

$$A_1 = \begin{bmatrix} \frac{r_t}{a_t} & -a_t \cos\theta_t & 0 & 0 & 0 & \frac{a_t e_t \sin\theta_t}{\sqrt{1-e_t^2}} \\ 0 & \frac{r_t \sin\theta_t}{1-e_t^2}(2 + e_t \cos\theta_t) & 0 & r_t & r_t \cos i_t & \frac{r_t}{(1-e_t^2)^{3/2}} \\ 0 & 0 & r_t \sin\theta_t & 0 & -r_t \cos\theta_t \sin\theta_t & 0 \end{bmatrix} \tag{3}$$

The variable Δx contains the difference in orbital elements between the chaser and the target spacecraft such that $\Delta x = x_c - x_t$, where the subscripts c and t denote the chaser and target respectively.

Schaub [32, p. 593-673] also derived equations for relative velocity in the LVLH reference frame; however, they are derived based on non-singular orbital elements.

The linearized equations relating relative orbital elements to relative velocity are herein derived by taking the time derivative of Eq. 1 shown below

$$\dot{\boldsymbol{\rho}} = \begin{bmatrix} \dot{x} & \dot{y} & \dot{z} \end{bmatrix}^T = \left(\frac{d}{dt} A_1 \right) \Delta x + A_1 \Delta \dot{x} \tag{4}$$

It will be shown in the following section that $\Delta \dot{x} = F \Delta x$, where F contains the combined keplerian and perturbing effects. The relative velocity in LVLH can be simplified as

$$\dot{\boldsymbol{\rho}} = \left(\begin{bmatrix} A_{21} & A_{22} \end{bmatrix} + A_1 F \right) \Delta x \tag{5}$$

where

$$A_{21} = \begin{bmatrix} \frac{\dot{r}_t}{a_t} & a_t \dot{\theta}_t \sin \theta_t & 0 \\ 0 & \frac{1}{1-e_t^2} [\dot{r}_t \sin \theta_t (2 + e_t \cos \theta_t) + & 0 \\ & \dot{\theta}_t \cos \theta_t r_t (2 + e_t \cos \theta_t) + & \\ & \sin \theta_t r_t (2 - e_t \dot{\theta}_t \sin \theta_t)] & \\ 0 & 0 & \dot{r}_t \sin \theta_t + r_t \dot{\theta}_t \cos \theta_t \end{bmatrix} \tag{6}$$

$$A_{22} = \begin{bmatrix} 0 & 0 & \frac{a_t e_t \dot{\theta}_t \cos \theta_t}{\sqrt{1-e_t^2}} \\ \dot{r}_t & \dot{r}_t \cos i_t & \frac{\dot{r}_t}{(1-e_t^2)^{3/2}} \\ 0 & -\dot{r}_t \cos \theta_t \sin \theta_t + r_t \dot{\theta}_t (\sin \theta_t + \cos \theta_t) & 0 \end{bmatrix} \tag{7}$$

The target's radial, radial rate of change and true anomaly rate magnitudes (r_t, $\dot{r}_t$, and $\dot{\theta}_t$) are calculated as follows

$$r_t = \frac{a_t(1 - e_t^2)}{1 + e_t \cos \theta_t} \tag{8}$$

$$\dot{r}_t = \sqrt{\frac{\mu}{a_t(1 - e_t^2)}} e_t \sin(\theta_t) \tag{9}$$

$$\dot{\theta}_t = \frac{\sqrt{\mu a_t(1 - e_t^2)}}{r_t^2} \tag{10}$$

where θ_t is the target's true anomaly.

Since the equations shown above are functions of the true anomaly, θ, a way of computing it is required. Gurfil and Kholshevnikov [12] proposed to numerically integrate for the time derivative of the true anomaly, but the purpose of this paper is to provide a fully analytical solution. Many solutions to obtain the true anomaly from the mean anomaly, eccentric anomaly and the orbit's eccentricity exist. Vallado illustrates many of these methods, including a method that uses modified Bessel functions of the first kind paired with the eccentricity and mean anomaly to solve for the true anomaly [37, p. 80-81]. Kuiack and Ulrich [23] modified Gurfil and Kholeshnikov's solution to include a analytical approximation for the true anomaly in terms of the eccentric anomaly. The simple recursive solution is given by

$$E = M + e \sin(M + e \sin(M + e \sin(M + ... + e \sin(M)))) \tag{11}$$

$$\cos\theta = \frac{\cos E - e}{1 - e\cos E} \qquad (12)$$

$$\sin\theta = \frac{\sqrt{1 - e^2}\sin E}{1 - e\cos E} \qquad (13)$$

$$\theta = \tan^{-1}\frac{\sin\theta}{\cos\theta} \qquad (14)$$

where E is the eccentric anomaly. This is a recursive solution based on the Newton-Raphson Iteration Technique [1] which implies an infinite series. Therefore, a term will become truncated based on the desired accuracy. The mean anomaly can be found by

$$M = M_0 + \dot{M}(t_f - t_0) \qquad (15)$$

$$\dot{M} = n = \sqrt{\frac{\mu}{a^3}} \qquad (16)$$

This formulation assumes a Keplerian orbit and one can incorporate perturbations by adding secular variations such that the target's orbital elements varies with time.

State Transition Matrix Formulation

This section presents the formulation used to derive the state transiton matrix that maps the states at a time t_f to the initial states at t_0, which is the most significant contribution of this paper. To first formulate the state transition matrix, the system dynamics must be defined by the derivative of the state vector, $\dot{x}$, as a function of the states

$$\dot{x} = \begin{bmatrix} \dot{a} & \dot{e} & \dot{i} & \dot{\omega} & \dot{\Omega} & \dot{M} \end{bmatrix}^T = f(x) \qquad (17)$$

and the function is the combination of keplerian and total perturbing effects considered represented by

$$f(x) = f_{kep}(x) + \sum f_{perturb}(x) \qquad (18)$$

where

$$f_{kep}(x) = \begin{bmatrix} 0 & 0 & 0 & 0 & 0 & n \end{bmatrix}^T \qquad (19)$$

$$f_{perturb}(x) = \begin{bmatrix} \dot{a}_{perturb} & \dot{e}_{perturb} & \dot{i}_{perturb} & \dot{\omega}_{perturb} & \dot{\Omega}_{perturb} & \dot{M}_{perturb} \end{bmatrix}^T \qquad (20)$$

The system dynamics can now be expressed in terms of relative orbital elements by taking the Jacobian of Eq. 17 as

$$\Delta\dot{x} = F(x)\Delta x \qquad (21)$$

where

$$F(x) = \left.\frac{\partial f(x)}{\partial x}\right|_{x=x_t} \qquad (22)$$

The system represented by Eq. 21 is a state-space representation of spacecraft relative dynamics based on equilibrium states x, or in this case the target's orbital elements. Depending on the dynamical representation given by Eq. 17, the system given by

Eq. 21 can either be linear time-varying (LTV) or time-invariant (LTI). The perturbing equations within Eq. 17 used to derive the Jacobian matrices is based on averaged models (over the true anomaly) of drag, gravity and third-body perturbations and as a result, the true anomaly does not appear in the equations for the Jacobian [24, 25, 30]. Therefore, the model represented by Eq. 21 can be assumed to be LTI since the elements of matrix $F(x)$ varies on the order of months or years (due to the variations in RAAN and argument of perigee). Since this paper explores the case of relative motion over relatively small periods (small periods being on the order of orbital periods, which equate to hours or days), the argument that the system is LTI holds, and it would have minimal effect on the accuracy of the model.

Now that the system dynamics have been defined, it can be linearized through a Taylor series expansion about the target's states such that

$$\Delta x_f = \left[I_{6\times6} + F(x)\Delta t + \frac{F^2(x)}{2!}\Delta t^2 + \frac{F^3(x)}{3!}\Delta t^3 ... \right] \Delta x_0 \qquad (23)$$

where $\Delta t = t_f - t_0$ and the Jacobian matrix $F(x)$ is evaluated at the target's initial states. The overall accuracy of the model can be improved by splitting the propagation in shorter time-steps and not using a fixed constant initial condition for the target, but this will not improve the accuracy by a significant amount. Furthermore, that would defeat the purpose of this paper, which is to formulate a model that is computationally efficient and can perform required computations with a single step. The Keplerian Jacobian is found as

$$F_{kep}(x) = \begin{bmatrix} 0 & 0 & 0 & 0 & 0 & 0 \\ 0 & 0 & 0 & 0 & 0 & 0 \\ 0 & 0 & 0 & 0 & 0 & 0 \\ 0 & 0 & 0 & 0 & 0 & 0 \\ 0 & 0 & 0 & 0 & 0 & 0 \\ -1.5n/a & 0 & 0 & 0 & 0 & 0 \end{bmatrix} \qquad (24)$$

Recently, Kuiack and Ulrich [23] developed a model which only includes the second zonal harmonic in terms of its secular and short periodic variations based off of Brouwer's [2] gravitational equations. Vinti [38] expanded on Brouwer's [2] and Kozai's [21] work to include the effects of the residual fourth zonal harmonic. In addition, an analytical relative dynamics for a J_2 perturbed elliptical orbit was formulated by Hamel and Lafontaine [14] but only included secular variations of RAAN, argument of perigee and mean anomaly. Liu [25] expanded on Brouwer's and Kozai's work to include secular variations of eccentricity and inclination, and concluded that their effects are small (about 0.5% more accurate). This paper uses the secular equations reformulated by Liu [25] as a basis to derive the gravitational field

Jacobian matrices $\boldsymbol{F}_J(\boldsymbol{x})$ for relative orbital elements. The Jacobian matrix is herein derived as

$$\boldsymbol{F}_J(\boldsymbol{x}) = \begin{bmatrix} 0 & 0 & 0 & 0 & 0 & 0 \\ F_J{}^{21} & F_J{}^{22} & F_J{}^{23} & F_J{}^{24} & 0 & 0 \\ F_J{}^{31} & F_J{}^{32} & F_J{}^{33} & F_J{}^{34} & 0 & 0 \\ F_J{}^{41} & F_J{}^{42} & F_J{}^{43} & 0 & 0 & 0 \\ F_J{}^{51} & F_J{}^{52} & F_J{}^{53} & 0 & 0 & 0 \\ F_J{}^{61} & F_J{}^{62} & F_J{}^{63} & 0 & 0 & 0 \end{bmatrix} \tag{25}$$

where the matrix elements are herein obtained as

$$\begin{aligned}
F_J{}^{21} = \; & \frac{1}{64a^8(e^2-1)^3 n} \Big[3R_E^3 \mu \sin(i)(144 J_3 a \cos(\omega) - 180 J_3 a \cos(\omega) \sin^2(i) \\
& - 144 J_3 a e^2 \cos(\omega)) + 165 J_2^2 R_E e \sin(2\omega) \sin^3(i) + 330 J_4 R_E e \sin(2\omega) \sin(i) \\
& + 180 J_3 a e^2 \cos(\omega) \sin^2(i) - 154 J_2^2 R_E e \sin(2\omega) \sin(i) \\
& - 385 J_4 R_E e \sin(2\omega) \sin^3(i) \Big]
\end{aligned} \tag{26}$$

$$\begin{aligned}
F_J{}^{22} = \; & -\frac{1}{32a^4(e^2-1)^3} \Big[3J_2^2 R_E^4 \sin(2\omega) \sin^2(i) n (15 \sin^2(i) - 14) \\
& + 15 J_4 R_E^4 \sin(2\omega) \sin^2(i) n (7 \sin^2(i) - 6) \Big] \\
& + \frac{1}{16a^4(e^2-1)^4} \Big[9 J_2^2 R_E^4 e^2 \sin(2\omega) \sin^2(i) n (15 \sin^2(i) - 14) - \\
& 45 J_4 R_E^4 e^2 \sin(2\omega) \sin^2(i) n (7 \sin^2(i) - 6) \Big] \\
& + \frac{3 J_3 R_E^3 e \cos(\omega) \sin(i) n (5 \sin^2(i) - 4)}{2a^3(e^2-1)^3}
\end{aligned} \tag{27}$$

$$\begin{aligned}
F_J{}^{23} = \; & -\frac{1}{(8a^4(e^2-1)^3)} \Big[3R_E^3 \cos(i) n (4 J_3 a \cos(\omega) - 15 J_3 a \cos(\omega) \sin^2(i) \\
& - 4 J_3 a e^2 \cos(\omega)) - 15 J_2^2 R_E e \sin(2\omega) \sin^3(i) + 15 J_4 R_E e \sin(2\omega) \sin(i) \\
& + 15 J_3 a e^2 \cos(\omega) \sin^2(i) + 7 J_2^2 R_E e \sin(2\omega) \sin(i) \\
& - 35 J_4 R_E e \sin(2\omega) \sin^3(i)) \Big]
\end{aligned} \tag{28}$$

$$\begin{aligned}
F_J{}^{24} = \; & \frac{1}{16a^4(e^2-1)^3} \Big[15 J_4 R_E^4 e \cos(2\omega) \sin^2(i) n (7 \sin^2(i) - 6) \\
& - 3 J_2^2 R_E^4 e \cos(2\omega) \sin^2(i) n (15 \sin^2(i) - 14) \Big] \\
& + \frac{3 J_3 R_E^3 \sin(i) \sin(\omega) n (5 \sin^2(i) - 4)}{8a^3(e^2-1)^2}
\end{aligned} \tag{29}$$

$$
\begin{aligned}
F_J{}^{31} = {} & -\frac{3R_E^3 e\mu}{128a^8(e^2-1)^4 n}\Big[360 J_3 a\cos^3(i)\cos(\omega) - 72 J_3 a\cos(i)\cos(\omega)\\
& +154 J_2^2 R_E e\sin(2i)\sin(2\omega) + 72 J_3 a e^2 \cos(i)\cos(\omega)\\
& -360 J_3 a e^2 \cos^3(i)\cos(\omega) + 330 J_4 R_E e\sin(2i)\sin(2\omega)\\
& + -330 J_2^2 R_E e\sin(2\omega)\cos(i)\sin^3(i) - 770 J_4 R_E e\sin(2\omega)\cos(i)\sin^3(i)\Big]
\end{aligned}
\tag{30}
$$

$$
\begin{aligned}
F_J{}^{32} = {} & \frac{1}{8a^4(e^2-1)^5}\Big[3 J_2^2 R_E^4 e^3 \sin(2i)\sin(2\omega)n(15\sin^2(i)-14)8a^4(e^2-1)^5\\
& +15 J_4 R_E^4 e^3 \sin(2i)\sin(2\omega)n(7\sin^2(i)-6)\Big]\\
& -\frac{1}{32a^4(e^2-1)^4}\Big[15 J_4 R_E^4 e\sin(2i)\sin(2\omega)n(7\sin^2(i)-6)\\
& -3 J_2^2 R_E^4 e\sin(2i)\sin(2\omega)n(15\sin^2(i)-14)\Big]\\
& -\frac{3 J_3 R_E^3 \cos(i)\cos(\omega)n(5\cos^2(i)-1)}{8a^3(e^2-1)^3}\\
& +\frac{9 J_3 R_E^3 e^2 \cos(i)\cos(\omega)n(5\cos^2(i)-1)}{4a^3(e^2-1)^4}
\end{aligned}
\tag{31}
$$

$$
\begin{aligned}
F_J{}^{33} = {} & \frac{1}{16a^4(e^2-1)^4}\Big[3R_E^3 e\cos(\omega)n(30 J_3 a\sin^3(i) - 28 J_3 a\sin(i)\\
& -30 J_3 a e^2 \sin^3(i) + 30 J_4 R_E e\sin(\omega) + 14 J_2^2 R_E e\sin(\omega) + 28 J_3 a e^2 \sin(i)\\
& -165 J_4 R_E e\sin^2(i)\sin(\omega) + 140 J_4 R_E e\sin^4(i)\sin(\omega)\\
& -73 J_2^2 R_E e\sin^2(i)\sin(\omega) + 60 J_2^2 R_E e\sin^4(i)\sin(\omega))\Big]
\end{aligned}
\tag{32}
$$

$$
\begin{aligned}
F_J{}^{34} = {} & \frac{3 J_3 R_E^3 e\cos(i)\sin(\omega)n(5\cos^2(i)-1)}{8a^3(e^2-1)^3}\\
& -\frac{1}{32a^4(e^2-1)^4}\Big[3 J_2^2 R_E^4 e^2 \cos(2\omega)\sin(2i)n(15\sin^2(i)-14)\\
& -15 J_4 R_E^4 e^2 \cos(2\omega)\sin(2i)n(7\sin^2(i)-6)\Big]
\end{aligned}
\tag{33}
$$

$$
\begin{aligned}
F_J{}^{41} = {} & -\frac{3R_E^2\mu}{256a^8(e^2-1)^4 n}\Big[3520 J_4 R_E^2 + 896 J_2 a^2 + 3960 J_4 R_E^2 e^2 - 1792 J_2 a^2 e^2\\
& +896 J_2 a^2 e^4 + 616 J_2^2 R_E^2 e^2 - 13640 J_4 R_E^2 \sin^2(i) - 495 J_2^2 R_E^2 e^2 \sin^4(i)\\
& +10780 J_4 R_E^2 \sin^4(i) - 1120 J_2 a^2 \sin^2(i) + 8360 J_2^2 R_E^2 \sin^2(i)\\
& -9790 J_2^2 R_E^2 \sin^4(i) - 13860 J_4 R_E^2 e^2 \sin^2(i) + 10395 J_4 R_E^2 e^2 \sin^4(i)\\
& +2240 J_2 a^2 e^2 \sin^2(i) - 1120 J_2 a^2 e^4 \sin^2(i) - 396 J_2^2 R_E^2 e^2 \sin^2(i)\Big]
\end{aligned}
\tag{34}
$$

$$F_J{}^{42} = -\frac{3R_E^2 en}{64a^4(e^2-1)^5}\Big[1640J_4R_E^2 + 256J_2a^2 + 56J_2^2R_E^2 + 1080J_4R_E^2e^2$$
$$-512J_2a^2e^2 + 256J_2a^2e^4 + 168J_2^2R_E^2e^2 - 6220J_4R_E^2\sin^2(i)$$
$$+4865J_4R_E^2\sin^4(i) - 320J_2a^2\sin^2(i) + 3004J_2^2R_E^2\sin^2(i)$$
$$-3605J_2^2R_E^2\sin^4(i) - 3780J_4R_E^2e^2\sin^2(i) + 2835J_4R_E^2e^2\sin^4(i)$$
$$+640J_2a^2e^2\sin^2(i) - 320J_2a^2e^4\sin^2(i) - 108J_2^2R_E^2e^2\sin^2(i)$$
$$-135J_2^2R_E^2e^2\sin^4(i)\Big] \tag{35}$$

$$F_J{}^{43} = -\frac{15J_4R_E^4}{n}\left[\frac{2\cos(i)\sin(i)(252e^2+248) - 4\cos(i)\sin^3(i)(189e^2+196)}{128a^4(e^2-1)^4}\right]$$
$$-3J_2^2R_E^4n\left[\frac{2\cos(i)\sin(i)(36e^2-760) + 4\cos(i)\sin^3(i)(45e^2+890)}{128a^4(e^2-1)^4}\right]$$
$$-\frac{15J_2R_E^2\cos(i)\sin(i)n}{2a^2(e^2-1)^2} \tag{36}$$

$$F_J{}^{51} = \frac{3R_E^2\mu\cos(i)}{64a^8(e^2-1)^4n}\Big[330J_4R_E^2 + 112J_2a^2 + 748J_2^2R_E^2 + 495J_4R_E^2e^2$$
$$-224J_2a^2e^2 + 112J_2a^2e^4 + 99J_2^2R_E^2e^2 - 770J_4R_E^2\cos^2(i)$$
$$-880J_2^2R_E^2\cos^2(i)^2 - 1155J_4R_E^2e^2\cos^2(i) - 55J_2^2R_E^2e^2\cos^2(i)\Big] \tag{37}$$

$$F_J{}^{52} = \frac{3R_E^2 e\cos(i)n}{16a^4(e^2-1)^5}\Big[32J_2a^2 - 220J_4R_E^2 - 44J_2^2R_E^2 - 180J_4R_E^2e^2$$
$$-64J_2a^2e^2 + 32J_2a^2e^4 + 12J_2^2R_E^2e^2 + 385J_4R_E^2\sin^2(i)$$
$$+325J_2^2R_E^2\sin^2(i) + 315J_4R_E^2e^2\sin^2(i) + 15J_2^2R_E^2e^2\sin^2(i)\Big] \tag{38}$$

$$F_J{}^{53} = \frac{3R_E^2\sin(i)n}{32a^4(e^2-1)^4}\Big[16J_2a^2 - 180J_4R_E^2 - 172J_2^2R_E^2 - 270J_4R_E^2e^2$$
$$-32J_2a^2e^2 + 16J_2a^2e^4 - 6J_2^2R_E^2e^2 + 210J_4R_E^2\sin^2(i) + 240J_2^2R_E^2\sin^2(i)$$
$$+315J_4R_E^2e^2\sin^2(i) + 15J_2^2R_E^2e^2\sin^2(i)\Big] \tag{39}$$

$$F_J{}^{61} = -\frac{1}{1024a^8(1-e^2)^{9/2}n}\Big[52800J_2^2R_E^4\mu\sin^2(i) - 69168J_2^2R_E^4\mu\sin(i)^4$$
$$+10560J_2^2R_E^4e^2\mu - 9240J_2^2R_E^4e^4\mu - 5376J_2R_E^2a^2\mu(e^2-1)^3$$
$$-51744J_2^2R_E^4e^2\mu\sin^2(i) + 35376J_2^2R_E^4e^2\mu\sin(i)^4 + 10824J_2^2R_E^4e^4\mu\sin^2(i)$$
$$+2607J_2^2R_E^4e^4\mu\sin(i)^4 + 15840J_4R_E^4e^2\mu(e^2-1)$$
$$+8064J_2R_E^2a^2\mu\sin^2(i)(e^2-1)^3 - 79200J_4R_E^4e^2\mu\sin(i)(e^2-1)$$
$$+69300J_4R_E^4e^2\mu\sin^2(i)(e^2-1)\Big] \tag{40}$$

$$
\begin{aligned}
F_J{}^{62} = &\; \frac{3J_2^2 R_E^4 n}{512 a^4 (1-e^2)^{9/2}} \Big[640e - 1120e^3 + \sin^4(i)(316e^3 + 2144e) \\
& - \sin^2(i)(-1312e^3 + 3136e) \Big] \\
& - \frac{9 J_2 R_E^2 e n (3\sin^2(i)^2 - 2)}{4 a^2 (1-e^2)^{5/2}} - \frac{45 J_4 R_E^4 e n (35\sin^2(i) - 40\sin(i) + 8)}{64 a^4 (1-e^2)^{7/2}} \\
& + \frac{27 J_2^2 R_E^4 e n}{512 a^4 (1-e^2)^{11/2}} \Big[\sin^4(i)(79e^4 + 1072e^2 - 2096) \\
& + \sin^2(i)(328e^4 - 1568e^2 + 1600) + 320e^2 - 280e^4 \Big] \\
& - \frac{315 J_4 R_E^4 e^3 n}{128 a^4 (1-e^2)^{9/2}} (35\sin^2(i) - 40\sin(i) + 8)
\end{aligned}
\tag{41}
$$

$$
\begin{aligned}
F_J{}^{63} = &\; \frac{3 J_2^2 R_E^4 n}{512 a^4 (1-e^2)^{9/2}} \Big[4\cos(i)\sin^3(i)(79e^4 + 1072e^2 - 2096) \\
& + 2\cos(i)\sin(i)(328e^4 - 1568e^2 + 1600) \Big] \\
& + 45 J_4 R_E^4 e^2 n \frac{40\cos(i) - 70\cos(i)\sin(i)}{128 a^4 (1-e^2)^{7/2}} - \frac{9 J_2 R_E^2 \cos(i)\sin(i) n}{2 a^2 (1-e^2)^{3/2}}
\end{aligned}
\tag{42}
$$

where J_2, J_3 and J_4 are the second, third and fourth zonal harmonics respectively, R_E is the mean radius of the Earth, μ is the gravitational constant of Earth and n is the mean orbital motion of the satellite.

The effects of third body perturbations on satellite orbits has been studied extensively in the past and continues to be in the present. Kozai [20] developed the first secular and long-periodic equations on the effects of luni-solar perturbations on a satellite's orbital elements based on the assumption that the distance of the satellite from the Earth was very small compared to the moon and that the moon's orbit is circular. Those equations were re-visited to include short periodic terms [22]. Smith [29, 34] extended Kozai's theory to include secular changes for a third body in an elliptical orbit and found that for NASA's Echo 1 mission, the perigee radius decreased as much as 100 meters over 25 days. Luni-solar effects on orbital elements were also developed by Cook [4] who also included the effects of solar radiation pressure, Kaula [18] and Giacagla [7] who also developed secular and periodic variations. Furthermore, Musen, et al. [28] expanded on Kozai's theory where it was observed that the third body perturbation causes the perigee height of a satellite to increase with periodic variations over long durations (20 km increase over approximately one month duration) due to third body effects on eccentricity. Recently, Domingos, et al. [6] and Prado [30], developed a simplified analytical model for a satellite's orbital elements based on the third body disturbing function expanded in Legendre polynomials up to fourth order. Specifically, the authors developed analytical model double

averaged the expanded disturbing function over the satellite's orbital period and then again over the third body's. The third body Jacobian matrix is derived in this work as

$$
\boldsymbol{F}_{3rd}(\boldsymbol{x}) = \begin{bmatrix} 0 & 0 & 0 & 0 & 0 & 0 \\ F_{3rd}^{21} & F_{3rd}^{22} & F_{3rd}^{23} & F_{3rd}^{24} & 0 & 0 \\ F_{3rd}^{31} & F_{3rd}^{32} & F_{3rd}^{33} & F_{3rd}^{34} & 0 & 0 \\ F_{3rd}^{41} & F_{3rd}^{42} & F_{3rd}^{43} & F_{3rd}^{44} & 0 & 0 \\ F_{3rd}^{51} & F_{3rd}^{52} & F_{3rd}^{53} & F_{3rd}^{54} & 0 & 0 \\ F_{3rd}^{61} & F_{3rd}^{62} & F_{3rd}^{63} & F_{3rd}^{64} & 0 & 0 \end{bmatrix} \tag{43}
$$

where the matrix elements are herein obtained as

$$
\begin{aligned}
F_{3rd}^{21} = \frac{45 e \mu K n'^2 (1-e^2)^{1/2}}{16384 a^4 a'^2 n} &\left[588 a^2 \sin(2\omega) + 294 a^2 e^2 \sin(2\omega) \right. \\
&+ 3087 a^2 e^2 \sin(4\omega) + 784 a^2 \cos(2i) \sin(2\omega) + 1024 a'^2 \sin(2\omega) \sin^2(i) \\
&\left. + 392 a^2 e^2 \cos(2i) \sin(2\omega) - 4116 a^2 e^2 \cos(2i) \sin(4\omega) \right]
\end{aligned} \tag{44}
$$

$$
\begin{aligned}
F_{3rd}^{22} = -\frac{15 K n'^2}{8192(1-e^2)^{1/2} a'^2 n} &\left[126 a^2 e^2 \sin(2\omega) - 252 a^2 \sin(2\omega) \right. \\
&- 3969 a^2 e^2 \sin(4\omega) + 504 a^2 e^4 \sin(2\omega) + 5292 a^2 e^4 \sin(4\omega) \\
&- 336 a^2 \cos(2i) \sin(2\omega) - 1024 a'^2 \sin(2\omega) \sin^2(i) + 168 a^2 e^2 \cos(2i) \sin(2\omega) \\
&+ 5292 a^2 e^2 \cos(2i) \sin(4\omega) + 672 a^2 e^4 \cos(2i) \sin(2\omega) \\
&\left. - 7056 a^2 e^4 \cos(2i) \sin(4\omega) + 2048 a'^2 e^2 \sin(2\omega) \sin^2(i) \right]
\end{aligned} \tag{45}
$$

$$
\begin{aligned}
F_{3rd}^{23} = -\frac{15 e K n'^2 (1-e^2)^{1/2}}{1024 a'^2 n} &\left[84 a^2 \sin(2i) \sin(2\omega) - 256 a'^2 \sin(2\omega) \cos(i) \sin(i) \right. \\
&\left. + 42 a^2 e^2 \sin(2i) \sin(2\omega) - 441 a^2 e^2 \sin(2i) \sin(4\omega) \right]
\end{aligned} \tag{46}
$$

$$
\begin{aligned}
F_{3rd}^{24} = {}&\frac{15 e K n'^2 \cos(2\omega) \sin^2(i)(1-e^2)^{1/2}}{4n} \\
&+ \frac{9 a^2 K n'^2 (1-e^2)^{1/2}}{65536 a'^2 n} \left[2e^3 \cos(2\omega)(4480 \cos^2(i) - 560) \right. \\
&- 4e^3 (2\cos^2(2\omega) - 1)(47040 \cos^2(i) - 41160) \\
&\left. + 2e \cos(2\omega)(8960 \cos^2(i) - 1120) \right]
\end{aligned} \tag{47}
$$

$$
\begin{aligned}
F_{3rd}^{31} = -\frac{45 e^2 K n'^2 \sin(2\omega) \cos(i)}{8192 a a'^2 \sin(i)(1-e^2)^{1/2} n} &\left[784 a^2 \cos^2(i) - 512 a'^2 \cos^2(i) - 98 a^2 \right. \\
&+ 512 a'^2 - 49 a^2 e^2 + 392 a^2 e^2 \cos^2(i) + 7203 a^2 e^2 \cos(2\omega) \\
&\left. - 8232 a^2 e^2 \cos(2\omega) \cos^2(i) \right]
\end{aligned} \tag{48}
$$

$$F_{3rd}{}^{32} = -\frac{15eKn'^2 \sin(2\omega)\cos(i)}{4096a'^2 \sin(i)(1-e^2)^{(3/2)}n}\Big[672a^2\cos^2(i) + 1024a'^2\sin^2(i) - 84a^2$$
$$-42a^2e^2 + 63a^2e^4 + 336a^2e^2\cos^2(i) - 504a^2e^4\cos^2(i)$$
$$+12348a^2e^2\cos(2\omega) - 9261a^2e^4\cos(2\omega) - 512a'^2e^2\sin^2(i)$$
$$-14112a^2e^2\cos(2\omega)\cos^2(i) + 10584a^2e^4\cos(2\omega)\cos^2(i)\Big] \tag{49}$$

$$F_{3rd}{}^{33} = -\frac{15e^2Kn'^2\sin(2\omega)}{4096a'^2(1-e^2)^{1/2}(\cos^2(i)-1)n}\Big[1008a^2\cos^2(i) - 672a^2\cos^4(i)$$
$$-1536a'^2\cos^2(i) + 1024a'^2\cos^4(i) - 42a^2 + 512a'^2 - 21a^2e^2$$
$$+504a^2e^2\cos^2(i) - 336a^2e^2\cos^4(i) + 3087a^2e^2\cos(2\omega)$$
$$-10584a^2e^2\cos(2\omega)\cos^2(i) + 7056a^2e^2\cos(2\omega)\cos^4(i)\Big] \tag{50}$$

$$F_{3rd}{}^{34} = -\frac{15e^2Kn'^2\cos(2\omega)\cos(i)\sin(i)}{4(1-e^2)^{1/2}n}$$
$$-\frac{9a^2Kn'^2\cos(i)}{65536a'^2\sin(i)(1-e^2)^{1/2}n}\Big[2e^4\cos(2\omega)(4480\cos^2(i) - 560)$$
$$+2e^2\cos(2\omega)(8960\cos^2(i) - 1120)$$
$$-4e^4(2\cos^2(2\omega) - 1)(47040\cos^2(i) - 41160)\Big] \tag{51}$$

$$F_{3rd}{}^{41} = \frac{9\mu Kn'^2}{16384a^4a'^2(1-e^2)^{1/2}n^3}\Big[54880a^2\cos^4(i) - 40320a^2\cos^2(i)$$
$$+5120a'^2\cos^2(i) - 980a^2\cos(2\omega) + 5120a'^2\cos(2\omega) + 3360a^2 - 1024a'^2$$
$$-36855a^2e^2 + 33495a^2e^4 + 1024a'^2e^2 + 15960a^2e^2\cos^2(i)$$
$$+68600a^2e^2\cos^4(i) + 12600a^2e^4\cos^2(i) - 41160a^2e^4\cos^4(i)$$
$$+980a^2e^4\cos(2\omega) - 5120a'^2e^2\cos(2\omega) + 72030a^2e^2\cos(2\omega)^2$$
$$-72030a^2e^4\cos(2\omega)^2 + 7840a^2\cos(2\omega)\cos^2(i) - 5120a'^2\cos(2\omega)\cos^2(i)$$
$$+ 62720a^2e^2\cos(2\omega)\cos^2(i) - 109760a^2e^2\cos(2\omega)\cos^4(i)$$
$$+23520a^2e^4\cos(2\omega)\cos^2(i) - 54880a^2e^4\cos(2\omega)\cos^4(i)$$
$$-82320a^2e^2\cos(2\omega)^2\cos^2(i) + 82320a^2e^4\cos(2\omega)^2\cos^4(i)\Big] \tag{52}$$

$$F_{3rd}{}^{42} = -\frac{3eKn'^2}{8192a'^2(1-e^2)^{(3/2)}n}\Big[3600a^2\cos^2(i) - 82320a^2\cos^4(i)$$

$$-5120a'^2\cos^2(i) + 420a^2\cos(2\omega) + 5120a'^2\cos(2\omega) - 61740a^2\cos(2\omega)^2$$

$$+30150a^2 - 1024a'^2 - 73215a^2e^2 + 43065a^2e^4 + 1024a'^2e^2$$

$$-14760a^2e^2\cos^2(i) + 99960a^2e^2\cos^4(i) + 16200a^2e^4\cos^2(i)$$

$$-52920a^2e^4\cos^4(i) - 1680a^2e^2\cos(2\omega) + 1260a^2e^4\cos(2\omega)$$

$$-5120a'^2e^2\cos(2\omega) + 154350a^2e^2\cos(2\omega)^2 - 92610a^2e^4\cos(2\omega)^2$$

$$-57120a^2\cos(2\omega)\cos^2(i) + 94080a^2\cos(2\omega)\cos^4(i)$$

$$+5120a'^2\cos(2\omega)\cos^2(i) + 70560a^2\cos(2\omega)^2\cos^2(i)$$

$$-13440a^2e^2\cos(2\omega)\cos^2(i) + 47040a^2e^2\cos(2\omega)\cos^4(i)$$

$$+30240a^2e^4\cos(2\omega)\cos^2(i) - 70560a^2e^4\cos(2\omega)\cos^4(i)$$

$$-35280a^2e^2\cos(2\omega)^2\cos^2(i) - 141120a^2e^2\cos(2\omega)^2\cos^4(i)$$

$$+105840a^2e^4\cos(2\omega)^2\cos^4(i)\Big] \tag{53}$$

$$F_{3rd}{}^{43} = \frac{15Kn'^2\cos(i)(\cos^2(i)-1)}{512a'^2\sin(i)(1-e^2)^{1/2}n}\Big[1176a^2\cos^2(i) + 84a^2\cos(2\omega)$$

$$-128a'^2\cos(2\omega) - 432a^2 + 128a'^2 + 171a^2e^2 + 135a^2e^4$$

$$+1470a^2e^2\cos^2(i) - 882a^2e^4\cos^2(i) + 672a^2e^2\cos(2\omega)$$

$$+252a^2e^4\cos(2\omega) - 882a^2e^2\cos(2\omega)^2 - 2352a^2e^2\cos(2\omega)\cos^2(i)$$

$$-1176a^2e^4\cos(2\omega)\cos^2(i) + 1764a^2e^4\cos(2\omega)^2\cos^2(i)\Big] \tag{54}$$

$$F_{3rd}{}^{44} = \frac{3Kn'^2\sin(2\omega)(5\cos^2(i) + 5e^2 - 5)}{4(1-e^2)^{1/2}n}$$

$$-\frac{9a^2Kn'^2(1-e^2)^{1/2}}{32768a'^2n}[2\sin(2\omega)(2240\cos(2i) + 1680)$$

$$+2e^2\sin(2\omega)(2240\cos(2i) + 1680) - 4e^2\sin(4\omega)(11760\cos(2i) - 8820)\Big]$$

$$-\frac{9a^2Kn'^2\cos(i)}{65536a'^2\sin(i)(1-e^2)^{1/2}n}\Big[2e^4\sin(2\omega)(2240\sin(2i) - 7840\sin(4i))$$

$$-4e^4\sin(4\omega)(11760\sin(2i) - 5880\sin(4i))$$

$$+2e^2\sin(2\omega)(4480\sin(2i) - 15680\sin(4i))\Big] \tag{55}$$

$$F_{3rd}{}^{51} = \frac{\mu K n'^2}{16384 a a'^2 \mu \sin(i)(1-e^2)^{1/2}n} \left[5040a^2 \sin(2i)(e^2-1) \right.$$
$$-9216a'^2 \sin(2i) + 17640a^2 \sin(4i)(e^2-1)$$
$$-13824a'^2 e^2 \sin(2i) + 25200a^2 e^2 \sin(2i)(e^2-1)$$
$$+88200a^2 e^2 \sin(4i)(e^2-1) + 9450a^2 e^4 \sin(2i)(e^2-1)$$
$$+33075a^2 e^4 \sin(4i)(e^2-1) + 35280a^2 e^2 \cos(2\omega)\sin(2i)(e^2-1)$$
$$-123480a^2 e^2 \cos(2\omega)\sin(4i)(e^2-1) + 17640a^2 e^4 \cos(2\omega)\sin(2i)(e^2-1)$$
$$-61740a^2 e^4 \cos(2\omega)\sin(4i)(e^2-1) - 92610a^2 e^4 \cos(4\omega)\sin(2i)(e^2-1)$$
$$\left. +46305a^2 e^4 \cos(4\omega)\sin(4i)(e^2-1) + 46080a'^2 e^2 \cos(2\omega)\cos(i)\sin(i) \right] \quad (56)$$

$$F_{3rd}{}^{52} = \frac{3eKn'^2 \cos(i)(5\cos(2\omega)-3)}{4(1-e^2)^{1/2}n} - \frac{3eKn'^2 \cos(i)(3e^2 - 5e^2\cos(2\omega)+2)}{8(1-e^2)^{(3/2)}n}$$
$$-\frac{9a^2 K n'^2 (1-e^2)^{1/2}}{65536a'^2 \sin(i)n} \left[3200e(2\sin(2i) + 7\sin(4i)) \right.$$
$$+4e^3(1200\sin(2i) + 4200\sin(4i)) + 2e\cos(2\omega)(4480\sin(2i) - 15680\sin(4i))$$
$$+4e^3\cos(2\omega)(2240\sin(2i) - 7840\sin(4i))$$
$$\left. -4e^3\cos(4\omega)(11760\sin(2i) - 5880\sin(4i)) \right] + \frac{9a^2 e K n'^2}{65536a'^2 \sin(i)(1-e^2)^{1/2}n} \times$$
$$\left[640\sin(2i) + 2240\sin(4i) + e^4(1200\sin(2i) + 4200\sin(4i)) \right.$$
$$+e^2(3200\sin(2i) + 11200\sin(4i)) + e^4\cos(2\omega)(2240\sin(2i) - 7840\sin(4i))$$
$$-e^4\cos(4\omega)(11760\sin(2i) - 5880\sin(4i))$$
$$\left. +e^2\cos(2\omega)(4480\sin(2i) - 15680\sin(4i)) \right] \quad (57)$$

$$F_{3rd}{}^{53} = \frac{3Kn'^2 \sin(i)(3e^2 - 5e^2\cos(2\omega)+2)}{8(1-e^2)^{1/2}n} - \frac{9a^2 K n'^2 (1-e^2)^{1/2}}{65536a'^2 \sin(i)n} \left[1280\cos(2i) \right.$$
$$+8960\cos(4i) + e^4(2400\cos(2i) + 16800\cos(4i))$$
$$+e^2(6400\cos(2i) + 44800\cos(4i)) + e^4\cos(2\omega)(4480\cos(2i) - 31360\cos(4i))$$
$$-e^4\cos(4\omega)(23520\cos(2i) - 23520\cos(4i))$$
$$\left. +e^2\cos(2\omega)(8960\cos(2i) - 62720\cos(4i)) \right] + \frac{9a^2 K n'^2 \cos(i)(1-e^2)^{1/2}}{(65536a'^2 \sin^2(i)n)} \times$$
$$\left[640\sin(2i) + 2240\sin(4i) + e^4(1200\sin(2i) + 4200\sin(4i)) \right.$$
$$+e^2(3200\sin(2i) + 11200\sin(4i)) + e^4\cos(2\omega)(2240\sin(2i) - 7840\sin(4i))$$
$$-e^4\cos(4\omega)(11760\sin(2i) - 5880\sin(4i))$$
$$\left. +e^2\cos(2\omega)(4480\sin(2i) - 15680\sin(4i)) \right] \quad (58)$$

$$
\begin{aligned}
F_{3rd}{}^{54} =\ & \frac{9a^2 K n'^2 (1-e^2)^{1/2}}{65536 a'^2 \sin(i)\, n} \Big[2e^4 \sin(2\omega)(2240 \sin(2i) - 7840 \sin(4i)) \\
& -4e^4 \sin(4\omega)(11760 \sin(2i) - 5880 \sin(4i)) \\
& +2e^2 \sin(2\omega)(4480 \sin(2i) - 15680 \sin(4i)) \Big] - \frac{15 e^2 K n'^2 \sin(2\omega)\cos(i)}{4(1-e^2)^{1/2} n}
\end{aligned} \tag{59}
$$

$$
\begin{aligned}
F_{3rd}{}^{61} =\ & -\frac{3\mu K n'^2}{16384 a^4 a'^2 n^3} \Big[211680 a^2 \sin^4(i) - 265440 a^2 \sin^2(i) - 6144 a'^2 \sin^2(i) \\
& -41160 a^2 \sin^2(\omega) + 68964 a^2 + 14336 a'^2 + 167685 a^2 e^2 + 25305 a^2 e^4 \\
& +6144 a'^2 e^2 - 474600 a^2 e^2 \sin^2(i) + 441000 a^2 e^2 \sin^4(i) - 840 a^2 e^4 \sin^2(i) \\
& +88200 a^2 e^4 \sin^4(i) + 6144 a'^2 e^2 \sin^2(i) - 41160 a^2 e^2 \sin^2(\omega) \\
& -123480 a^2 e^2 \sin^4(\omega) + 82320 a^2 e^4 \sin^2(\omega) - 123480 a^2 e^4 \sin^4(\omega) \\
& +47040 a^2 \sin^2(i) \sin^2(\omega) - 15360 a'^2 \sin^2(i) \sin^2(\omega) \\
& -799680 a^2 e^2 \sin^2(i) \sin^2(\omega) + 987840 a^2 e^2 \sin^2(i) \sin^4(\omega) \\
& -940800 a^2 e^4 \sin^2(i) \sin^2(\omega) + 987840 a^2 e^4 \sin^2(i) \sin^4(\omega) \\
& -15360 a'^2 e^2 \sin^2(i) \sin^2(\omega) \Big]
\end{aligned} \tag{60}
$$

$$
\begin{aligned}
F_{3rd}{}^{62} =\ & -\frac{3 e K n'^2}{4096 a'^2 n} \Big[63000 a^2 \sin^4(i) - 67800 a^2 \sin^2(i) + 2048 a'^2 \sin^2(i) \\
& -5880 a^2 \sin^2(\omega) - 17640 a^2 \sin^4(\omega) + 23955 a^2 + 2048 a'^2 + 7230 a^2 e^2 \\
& -240 a^2 e^2 \sin^2(i) + 25200 a^2 e^2 \sin^4(i) + 23520 a^2 e^2 \sin^2(\omega) \\
& -35280 a^2 e^2 \sin^4(\omega) - 114240 a^2 \sin^2(i) \sin^2(\omega) + 141120 a^2 \sin^2(i) \sin^4(\omega) \\
& -5120 a'^2 \sin^2(i) \sin^2(\omega) - 268800 a^2 e^2 \sin^2(i) \sin^2(\omega) \\
& +282240 a^2 e^2 \sin^2(i) \sin^4(\omega) \Big]
\end{aligned} \tag{61}
$$

$$
\begin{aligned}
F_{3rd}{}^{63} =\ & \frac{3 K n'^2}{2048 a'^2 n} \Big[1080 a^2 \sin(2i) + 3780 a^2 \sin(4i) + 1792 a'^2 \sin(2i) \\
& +2250 a^2 e^2 \sin(2i) + 7875 a^2 e^2 \sin(4i) + 450 a^2 e^4 \sin(2i) + 1575 a^2 e^4 \sin(4i) \\
& +768 a'^2 e^2 \sin(2i) + 840 a^2 \cos(2\omega) \sin(2i) - 2560 a'^2 \cos(i) \cos(\omega)^2 \sin(i) \\
& +3360 a^2 e^2 \cos(2\omega) \sin(2i) - 4410 a^2 e^2 \cos(4\omega) \sin(2i) \\
& +840 a^2 e^4 \cos(2\omega) \sin(2i) - 4410 a^2 e^4 \cos(4\omega) \sin(2i) \\
& -2560 a'^2 e^2 \cos(i) \cos(\omega)^2 \sin(i) \Big]
\end{aligned} \tag{62}
$$

$$
\begin{aligned}
F_{3rd}{}^{64} = {} & \frac{9a^2 K n'^2}{8192 a'^2 n} \Big[2e^4 \sin(2\omega)(1120\cos(2i) + 840) \\
& + 2e^2 \sin(2\omega)(2240\cos(2i) + 1680) - 4e^4 \sin(4\omega)(5880\cos(2i) - 4410) \Big] \\
& + \frac{K n'^2 \cos(\omega) \sin^2(i) \sin(\omega)(15e^2 + 15)}{4n} \\
& - \frac{9a^2 K n'^2 (e^2 - 1)}{32768 a'^2 n} \big[2\sin(2\omega)(2240\cos(2i) + 1680) \\
& + 2e^2 \sin(2\omega)(2240\cos(2i) + 1680) - 4e^2 \sin(4\omega)(11760\cos(2i) - 8820) \big] (63)
\end{aligned}
$$

where $K = m'/(m' + m_0)$, m' is the mass of the third body, m_0 is the mass of the central body, n' is the mean orbital motion of the third body and a' is semi-major axis of the third body.

Although atmospheric drag is extensively studied, an exact or accurate model is yet to exist. One of the main reasons is the fact that density is difficult to model mainly due to the effects of solar wind activity on the atmosphere. However, analytical approximations of the effects of drag on orbital elements exist in literature based on the exponential model for density. The first analytical model was formulated by Izsak [17] where the effects were separated in terms of periodic and secular variations. Xu et al. [10] and Watson et al. [39] also developed an analytical solution for drag, while Danielson [5] developed a semi-analytic solution and Martinusi et al. [27] developed a first order accurate analytical solution. In addition, Lawden formulated secular variations of all orbital elements except mean anomaly due to atmospheric drag [24]. The drag Jacobian matrix is herein derived, based on Lawden's model, as

$$
\boldsymbol{F}_{Drag}(\boldsymbol{x}) =
\begin{bmatrix}
F_{Drag}{}^{11} & F_{Drag}{}^{12} & F_{Drag}{}^{13} & 0 & 0 & 0 \\
F_{Drag}{}^{21} & F_{Drag}{}^{22} & F_{Drag}{}^{23} & 0 & 0 & 0 \\
F_{Drag}{}^{31} & F_{Drag}{}^{32} & F_{Drag}{}^{33} & F_{Drag}{}^{34} & 0 & 0 \\
F_{Drag}{}^{41} & F_{Drag}{}^{42} & F_{Drag}{}^{43} & F_{Drag}{}^{44} & 0 & 0 \\
F_{Drag}{}^{51} & F_{Drag}{}^{52} & F_{Drag}{}^{53} & F_{Drag}{}^{54} & 0 & 0 \\
0 & 0 & 0 & 0 & 0 & 0
\end{bmatrix}
\tag{64}
$$

with

$$
\begin{aligned}
F_{Drag}{}^{11} = {} & -\frac{1}{8Hm(e+1)^{1/2}} \Big[C_D A a \rho \, exp(-c)(Hn(e+1)^{1/2} - 2aen(e+1)^{1/2} \\
& - 8H\omega_E \cos(i)(1-e)^{3/2} + 4ae\omega_E \cos(i)(1-e)^{3/2}) \times \\
& (4B_0 + 8B_1 e + 3B_0 e^2 + 3B_1 e^3 + 3B_2 e^2 + B_3 e^3) \Big]
\end{aligned}
\tag{65}
$$

$$F_{Drag}{}^{12} = \frac{1}{Hm(e+1)^{1/2}}\left[C_D A a^3 \rho exp(-c)(n(e+1)^{1/2} - 2\omega_E \cos(i)(1-e)^{3/2})\right.$$
$$\times (B_0 + 2B_1 e + 0.75 B_0 e^2 + 0.75 B_1 e^3 + 0.75 B_2 e^2 + 0.25 B_3 e^3)\Big]$$
$$-\frac{1}{m(e+1)^{1/2}}\left[C_D A a^2 \rho exp(-c)(n(e+1)^{1/2} - 2\omega_E \cos(i)(1-e)^{3/2})\right.$$
$$\times (2B_1 + 1.5 B_0 e + 1.5 B_2 e + 2.5 B_1 e^2 + 0.75 B_3 e^2\Big]$$
$$-\frac{1}{m(e+1)^{3/2}}\left[2C_D A a^2 \rho \omega_E exp(-c)\cos(i)(1-e)^{1/2}(e+2)\times\right.$$
$$(B_0 + 2B_1 e + 0.75 B_0 e^2 + 0.75 B_1 e^3 + 0.75 B_2 e^2 + 0.25 B_3 e^3)\Big] \qquad (66)$$

$$F_{Drag}{}^{13} = -\frac{2C_D A a^2 \rho \omega_E exp(-c)\sin(i)(1-e)^{3/2}}{m(e+1)^{1/2}} \times$$
$$\left[(B_0 + 2B_1 e + (3e^2(B_0 + B_2))/4 + (e^3(3B_1 + B_3))/4)\right] \qquad (67)$$

$$F_{Drag}{}^{21} = \frac{C_D A \rho exp(-c)}{32 Hm(e+1)^{1/2}}\left(Hn(e+1)^{1/2} + 2aen(e+1)^{1/2}\right.$$
$$+4H\omega_E \cos(i)(1-e)^{3/2} - 4ae\omega_E \cos(i)(1-e)^{3/2}\Big) \times$$
$$\left[(16B_1 + 8B_0 e + 8B_2 e - 5B_0 e^3 - 10B_1 e^2 - 4B_2 e^3 - 2B_3 e^2 + B_4 e^3)\right] \qquad (68)$$

$$F_{Drag}{}^{22} = \frac{C_D A a \rho exp(-c)(n(e+1)^{1/2} - 2\omega_E \cos(i)(1-e)^{3/2})}{m(e+1)^{1/2}} \times$$
$$\left[1.25 B_1 e - 0.5 B_2 - 0.5 B_0 + 0.25 B_3 e + \frac{15}{16} B_0 e^2\right.$$
$$\left. +0.75 B_2 e^2 - \frac{3}{16}3 B_4 e^2\right] + \frac{C_D A a^2 \rho exp(-c)}{Hm(e+1)^{1/2}}\left(n(e+1)^{1/2}\right.$$
$$\left. -2\omega_E \cos(i)(1-e)^{3/2}\right)\left[B_1 + 0.5 B_0 e + 0.5 B_2 e - \frac{3}{16} B_0 e^3\right.$$
$$\left. -\frac{5}{8} B_1 e^2 - 0.25 B_2 e^3 - 0.125 B_3 e^2 + \frac{1}{16} B_4 e^3\right] - \frac{2C_D A a \rho \omega_E exp(-c)}{m(e+1)^{3/2}} \times$$
$$\left(\cos(i)(1-e)^{1/2}(e+2)\right)\left[B_1 + 0.5 B_0 e + 0.5 B_2 e - \frac{5}{16} B_0 e^3 - \frac{5}{8}5 B_1 e^2\right.$$
$$\left. -0.25 B_2 e^3 - 0,125 B_3 e^2 + \frac{1}{16} B_4 e^3\right] \qquad (69)$$

$$F_{Drag}{}^{23} = -\frac{2C_D A a \rho \omega_E exp(-c)\sin(i)(1-e)^{3/2}}{m(e+1)^{1/2}}\left[B_1 - 0.125 e^2(5B_1 + B_3)\right.$$
$$\left. -\frac{1}{16} e^3(5B_0 + 4B_2 - B_4) + 0.5e(B_0 + B_2)\right] \qquad (70)$$

$$F_{Drag}{}^{31} = \frac{C_D A \rho \omega_E \exp(-c)}{16 H a^3 m n^3 \left[1 - (2\omega_E \cos(i)(1-e)^{3/2})/(n(e+1)^{1/2}))^{1/2}\right](e+1)^{1/2}}$$

$$\times \left[7 H \mu \omega_E \sin(2i)(1-e)^{3/2} - 4 H a^3 \sin(i) n^3 (e+1)^{1/2}\right.$$

$$+ 4 a^4 e \sin(i) n^3 (e+1)^{1/2} - 4 a e \mu \omega_E \sin(2i)(1-e)^{3/2}\Big] \times$$

$$[B_0 - 2 B_1 e + B_2 \cos(2\omega) - 2 B_1 e \cos(2\omega)] \tag{71}$$

$$F_{Drag}{}^{32} = \frac{C_D A a \rho \omega_E \exp(-c) \sin(i)}{4m} \left[1 - \frac{(2\omega_E \cos(i)(1-e)^{3/2})}{(n(e+1)^{1/2})^{1/2}}\right] \times$$

$$[2 B_1 + 2 B_1 \cos(2\omega)] + \frac{C_D A a^2 \rho \omega_E \exp(-c) \sin(i)}{4 H m} \times$$

$$\left[1 - \frac{(2\omega_E \cos(i)(1-e)^{3/2})}{(n(e+1)^{1/2})^{1/2}}\right][B_0 - 2 B_1 e + \cos(2\omega)(B_2 - 2 B_1 e)]$$

$$- \frac{C_D A a \rho \omega_E \exp(-c) \sin(i)}{8m \left[1 - \frac{(2\omega_E \cos(i)(1-e)^{3/2})}{(n(e+1)^{1/2})^{1/2}}\right]} \left[\frac{3\omega_E \cos(i)(1-e)^{1/2}}{n(e+1)^{1/2}}\right.$$

$$+ \frac{\omega_E \cos(i)(1-e)^{3/2}}{n(e+1)^{3/2}}\right][B_0 - 2 B_1 e + \cos(2\omega)(B_2 - 2 B_1 e)] \tag{72}$$

$$F_{Drag}{}^{33} = -\frac{C_D A a \rho \omega_E \exp(-c)}{4 m n Q^{0.5} (e+1)^{1/2}} \left[\cos(i) n (e+1)^{1/2} - 2\omega_E \cos^2(i)(1-e)^{3/2}\right.$$

$$+ \omega_E \sin^2(i)(1-e)^{3/2}\Big][B_0 - 2 B_1 e + B_2 \cos(2\omega) - 2 B_1 e \cos(2\omega)] \tag{73}$$

$$F_{Drag}{}^{34} = \left[C_D A a \rho \omega_E \sin(2\omega) \exp(-c) \sin(i) Q^{0.5}(B_2 - 2 B_1 e)\right]/(2m) \tag{74}$$

$$F_{Drag}{}^{41} = \frac{C_D A \rho \omega_E \sin(2\omega) \exp(-c) \cos(i)(B_2 - 2 B_1 e)}{8 H a^3 m n^3 \left[1 - (2\omega_E \cos(i)(e+1)^{3/2})/(n(e+1)^{1/2})\right]^{1/2}(e+1)^{1/2}} \times$$

$$\left(2 H a^3 n^3 (e+1)^{1/2} - 2 a^4 e n^3 (e+1)^{1/2} - 7 H \mu \omega_E \cos(i)(e+1)^{3/2}\right.$$

$$+ 4 a e \mu \omega_E \cos(i)(e+1)^{3/2}\Big) \tag{75}$$

$$F_{Drag}{}^{42} = \frac{C_D A a \rho \omega_E \sin(2\omega) \exp(-c) \cos(i)(B_2 - 2 B_1 e)}{8 m Q^{0.5}} \left(\frac{3\omega_E \cos(i)(1-e)^{1/2}}{n(e+1)^{1/2}}\right.$$

$$+ \frac{\omega_E \cos(i)(1-e)^{3/2}}{n(e+1)^{3/2}}\right) - \frac{B_1 C_D A a \rho \omega_E \sin(2\omega) \exp(-c) \cos(i) Q^{0.5}}{2m}$$

$$- C_D A a^2 \rho \omega_E \sin(2\omega) \exp(-c) \left[\cos(i) Q^{0.5}(B_2 - 2 B_1 e)\right]/(4 H m) \tag{76}$$

$$F_{Drag}{}^{43} = -\frac{C_D A a \rho \omega_E \sin(2\omega) \exp(-c) \sin(i)(B_2 - 2 B_1 e)}{4 m n Q^{0.5}(e+1)^{1/2}} \left[n(e+1)^{1/2}\right.$$

$$- 3\omega_E \cos(i)(1-e)^{3/2}\Big] \tag{77}$$

$$F_{Drag}{}^{44} = C_D A a \rho \omega_E \cos(2\omega) exp(-c) \cos(i) Q^{0.5}(B_2 - 2B_1 e)/(2m) \tag{78}$$

$$
\begin{aligned}
F_{Drag}{}^{51} = &-\frac{C_D A \rho \omega_E \sin(2\omega) exp(-c)(B_2 - 2B_1 e)}{8 H a^3 m n^3 Q^{0.5}(e+1)^{1/2}} \Big[2 H a^3 n^3 (e+1)^{1/2} \\
&-2 a^4 e n^3 (e+1)^{1/2} - 7 H \mu \omega_E \cos(i)(1-e)^{3/2} \\
&+4 a e \mu \omega_E \cos(i)(1-e)^{3/2} \Big]
\end{aligned}
\tag{79}
$$

$$
\begin{aligned}
F_{Drag}{}^{52} = &\frac{B_1 C_D A a \rho \omega_E \sin(2\omega) exp(-c) Q^{0.5}}{2m} \\
&+\frac{C_D A a^2 \rho \omega_E \sin(2\omega) exp(-c) Q^{0.5}(B_2 - 2B_1 e)}{4 H m} \\
&-\frac{C_D A a \rho \omega_E \sin(2\omega) exp(-c)(B2 - 2B1e)}{8m Q^{1/2}} \times \\
&\left[\frac{3 \omega_E \cos(i)(1-e)^{1/2}}{n(e+1)^{1/2}} + \frac{\omega_E \cos(i)(1-e)^{3/2}}{n(e+1)^{3/2}} \right]
\end{aligned}
\tag{80}
$$

$$F_{Drag}{}^{53} = -\frac{C_D A a \rho \omega_E^2 \sin(2\omega) exp(-c)}{\left[4mn Q^{0.5}(e+1)^{1/2} \right]} \sin(i)(B_2 - 2B_1 e)(1-e)^{3/2} \tag{81}$$

$$F_{Drag}{}^{54} = -C_D A a \rho \omega_E \cos(2\omega) exp(-c) Q^{1/2}(B_2 - 2B_1 e)/(2m) \tag{82}$$

where ω_E is angular velocity of Earth. The density at the perigee ρ, modified Bessel function of the first kind B_j with argument c and the constants c, Q and δ are given by

$$\rho = \rho_0 \exp(-\frac{h_p - h_0}{H}) \tag{83}$$

$$h_p = \bar{a}(1 - \bar{e}) - R_E \tag{84}$$

$$B_j(c) = \left(\frac{c}{2}\right)^j \sum_{k=0}^{\infty} \frac{\left(\frac{c}{2}\right)^{2k}}{k! \Gamma(j+k+1)} \tag{85}$$

$$c = \frac{\bar{a}\bar{e}}{H} \tag{86}$$

$$Q = 1 - \frac{2\omega_E (1-\bar{e})^{1.5}}{\bar{n}\sqrt{1+\bar{e}}} \cos(\bar{i}) \tag{87}$$

$$\delta = \frac{QAC_D}{m} \tag{88}$$

where ρ_0 is the atmospheric density in kg/m^3 and H is the scale height at a reference altitude h_0, h_p is altitude of perigee, Q is the factor for rotation of Earth's atmosphere (between 0.9-1.1), A is exposed area in m^2 to the direction of fluid flow and C_D is the coefficient of drag and m is mass of the spacecraft in kg.

Terminal-Point Guidance Law

This section presents the procedure, summarized in steps, of a terminal-point (or back-propagation) guidance law by using the new STM formulation developed in the previous sections. In most formation flying applications, the desired relative motion at some point later in time is known. Taking these conditions and back-propagating through the previously presented equations, the ideal initial motion of the chaser spacecraft may be calculated. That is, the set of initial relative orbital elements which will result in the desired formation at the final time can be calculated. This should result in reduced fuel consumption, as instead of forcing the chaser to track some arbitrary trajectory until a specific relative motion is achieved, the chaser is initially placed onto a natural trajectory that considers orbital perturbations. In other words, a set of initial conditions can be calculated such that the chaser spacecraft naturally drifts without the use of actuation into a desired final formation. The steps are as follows:

1. A set of Keplerian osculating orbital elements are first initialized for the target: $[a_{t_0}, e_{t_0}, i_{t_0}, \omega_{t_0}, \Omega_{t_0}, \theta_{t_0}]^T$ such that the Jacobian matrices are evaluated as:

$$F(x) = F_{kep}(x) + F_J(x) + F_{3rd}(x) + F_{Drag}(x) \tag{89}$$

2. Select the desired final time, Δt, at which the chaser is to drift into the desired final LVLH coordinates, ρ_f and $\dot{\rho}_f$.

3. The desired relative orbital elements, Δx_f can be found using Eqs. 2-16 and the following equation

$$\Delta x_f = \begin{bmatrix} A_{11} & A_{12} \\ A_{21} & A_{22} \end{bmatrix}^{-1} \begin{bmatrix} \rho_f \\ \dot{\rho}_f \end{bmatrix} \tag{90}$$

4. Finally, using Eq. 23, the initial relative orbital elements are found with a single step:

$$\Delta x_0 = \left[I_{6 \times 6} + F(x) \Delta t \right]^{-1} \Delta x_f \tag{91}$$

Numerical Simulations

This section presents a comparison of results obtained using the equations developed in this paper against a numerical propagator that integrates the exact nonlinear differential equations of motion in $\mathcal{F}_I$ to verify the accuracy of the model. The numerical propagator integrates the inertial two-body equation of motion to which the inertial perturbing accelerations due to gravitational field by expanding the gravitational potential function up to degree and order 180, third body effects of the sun, moon and solar system planets, ocean and solid Earth tidal effects, relativity, solar radiation pressure, and drag were added then converted from $\mathcal{F}_I$ to $\mathcal{F}_L$. The developed STM was applied to both the Proba-3 mission and fictitious mission involving a chaser spacecraft in formation around the decommissioned Alouette-2 communication satellite. Additionally, the terminal-point guidance method presented in this paper was applied to Alouette-2 for rendevous formation, for which a sensitivity analysis by

varying the drift time was performed. For all simulations, the osculating orbital elements for Alouette-2 and Proba-3 were respectively initialized as $a = 7947$ km, $e = 0.134$, $i = 79.8°$, $\omega = 151.9°$, $\Omega = 348.3°$, and $\theta = 0°$ and $a = 36944$ km, $e = 0.811$, $i = 59.0°$, $\omega = 188°$, $\Omega = 84.0°$, and $\theta = 0°$, respectively.

Figures 1, 2, 3 and 4 show the results for the Proba-3 and Alouette-2 cases using the new STM formulation, where two simulations with initial relative orbital elements initialized as $\Delta x_0 = [0, 5 \times 10^{-4}, 0, 0, 0, 0]^T$ and $\Delta x_0 = [0, 5 \times 10^{-4}, 0.1°, 0.1°, -0.1°, -0.1°]^T$, respectively, for both cases. The Alouette-2 case shows a growth in error in all directions, with significant growth in the cross-track direction, when observing Figs. 1 and 2. When comparing Figs. 3 and 4, the in-plane errors remained nearly the same whereas the cross-track errors increased from near 100 meters to just below 15000 meters which has minimal effects on accuracy when taking into account the relative distances involved. In both the Alouette-2 and Proba-3 cases, the results show that the solution maintains accuracy for an arbitrary eccentric orbit and large separations distances.

Figures 5, 6, 7, 8, 9, 10, 11, 12 and 13 show a sensitivity analysis by varying eccentricity and inclination of the proba-3 case with the same relative orbital elements condition of Fig. 4. The errors associated with the analytical model decrease as eccentricity or inclination decrease when observing the figures. Specifically, the results show that at the end of each orbit (i.e. at the perigee after each orbital period), the errors associated with the analytical model increases sharply which can be seen when comparing the figures with eccentricity variation. This is caused by the conversion of mean anomaly to true anomaly through the eccentric anomaly, which specifically affects the matrix that maps the propagated relative orbital elements to the cartesian coordinates in LVLH. However, the errors remain minimal and insignificant during
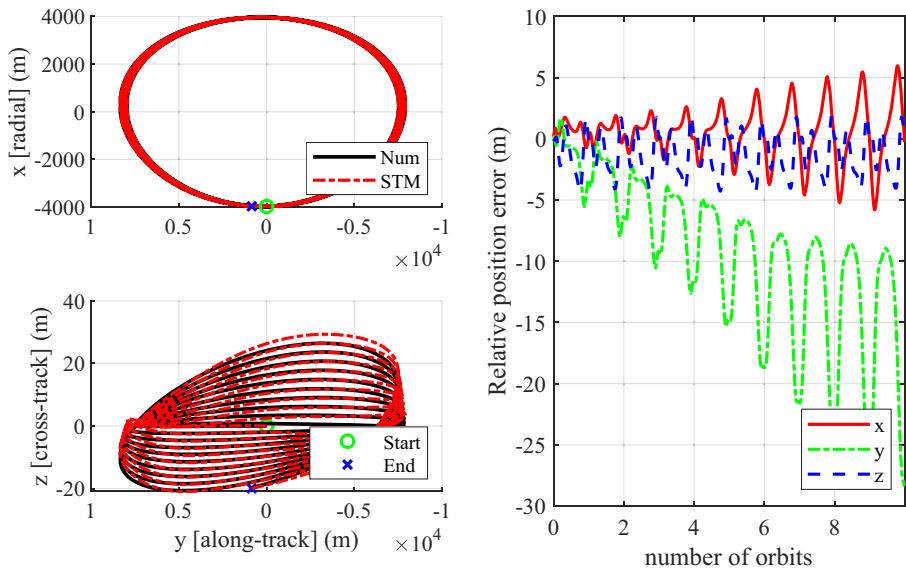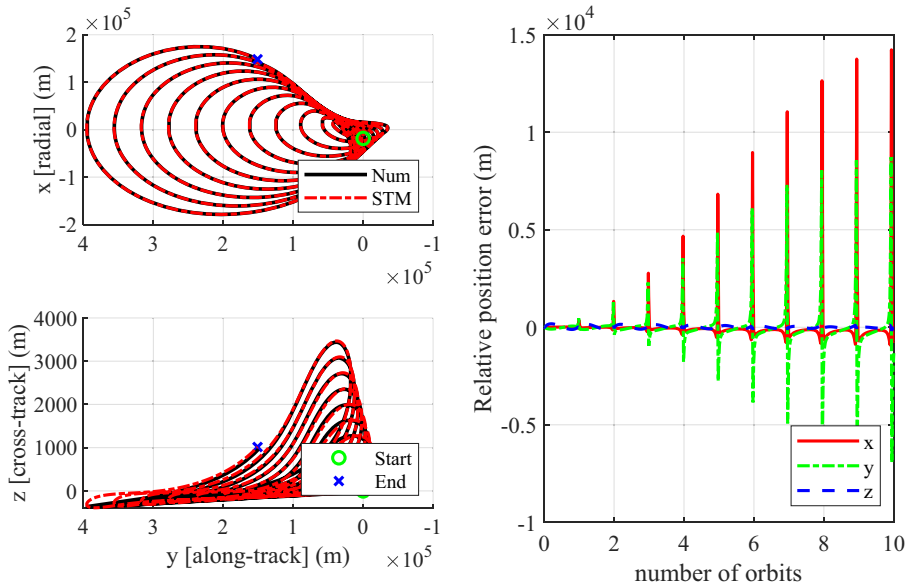

**Fig. 1** Alouette-2: STM for $\Delta x_0 = [0, 5 \times 10^{-4}, 0, 0, 0, 0]^T$
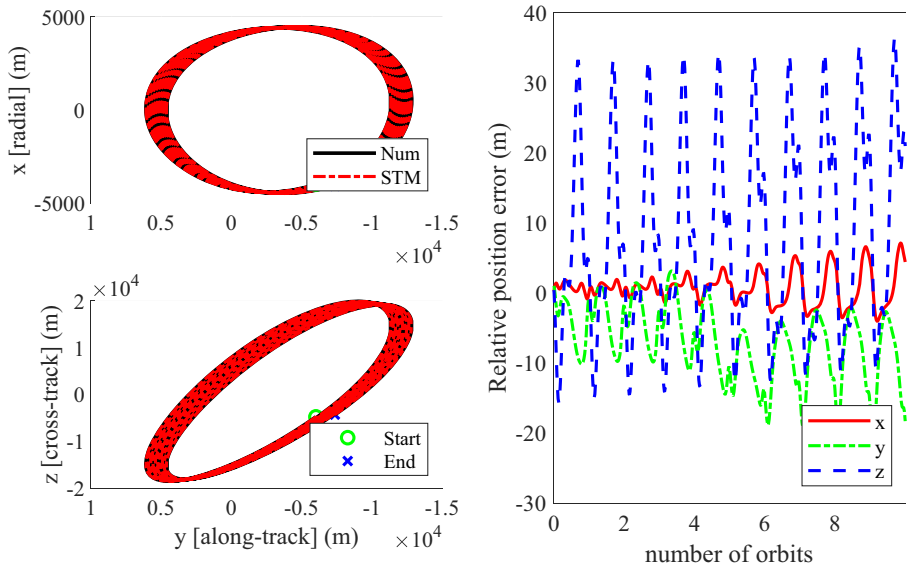
**Fig. 2** Alouette-2: STM for $\Delta x_0 = [0, 5 \times 10^{-4}, 0.1°, 0.1°, -0.1°, -0.1°]^T$

the time in between perigee passages, and in addition, the errors overall are minimal when observing the relative motion in LVLH. Furthermore, the decrease in error associated with the reduction in inclination is caused by the fact that solar radiation
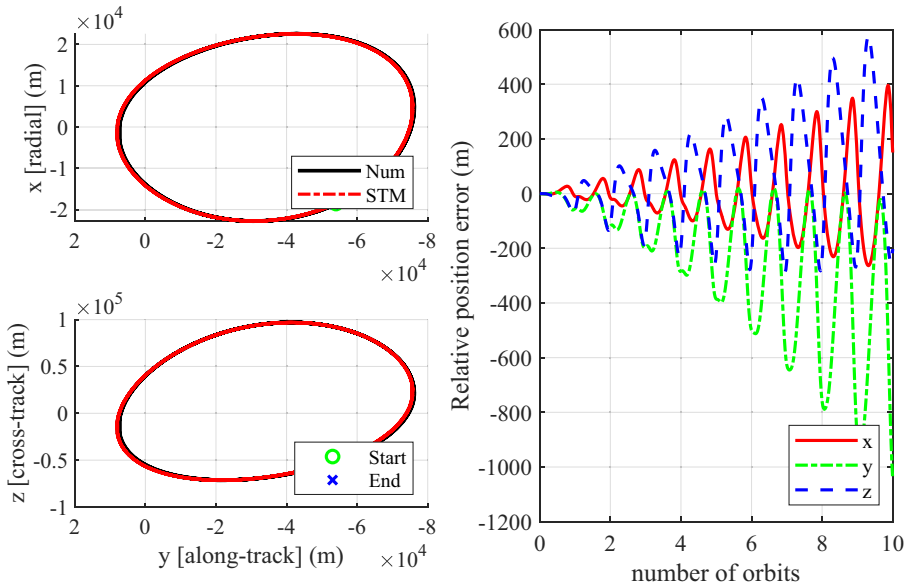

Fig. 3 Proba-3: STM for $\Delta x_0 = [0, 5 \times 10^{-4}, 0, 0, 0, 0]^T$
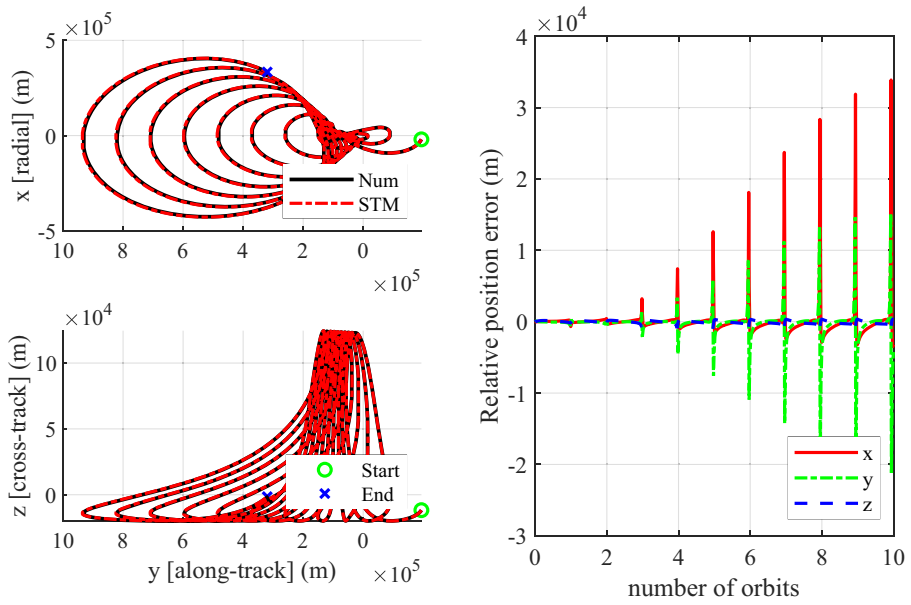
Fig. 4 Proba-3: STM for $\Delta x_0 = [0, 5 \times 10^{-4}, 0.1°, 0.1°, -0.1°, -0.1°]^T$
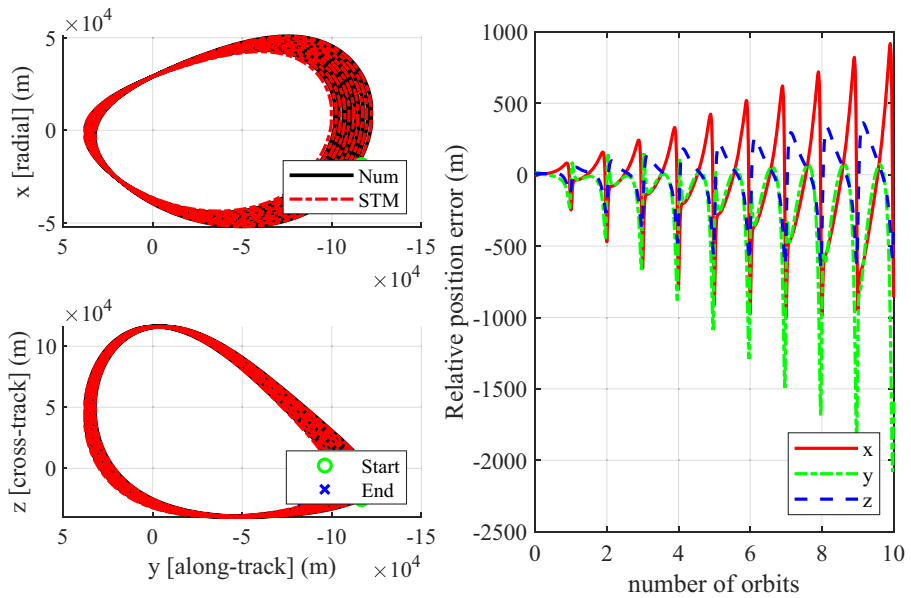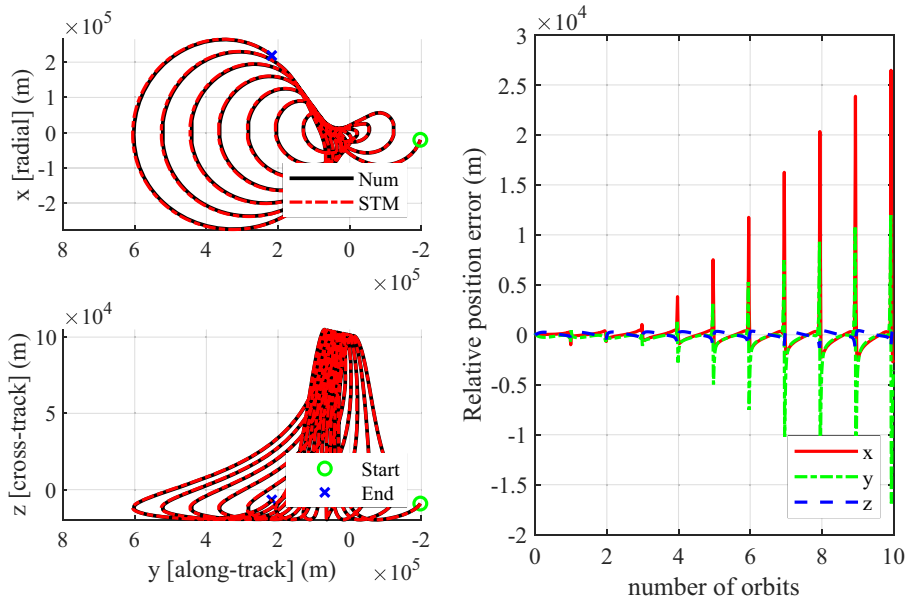

Fig. 5 Proba-3: STM for $e = 0.6$, $\Delta x_0 = [0, 5 \times 10^{-4}, 0.1°, 0.1°, -0.1°, -0.1°]^T$
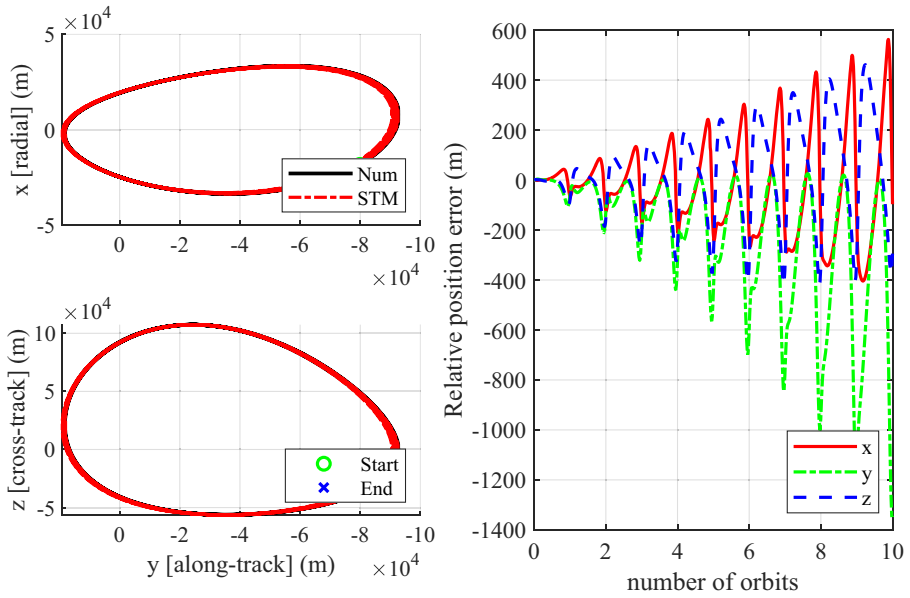
Fig. 6 Proba-3: STM for $e = 0.4$, $\Delta \boldsymbol{x}_0 = [0, 5 \times 10^{-4}, 0.1°, 0.1°, -0.1°, -0.1°]^T$

Fig. 7 Proba-3: STM for $e = 0.2$, $\Delta \boldsymbol{x}_0 = [0, 5 \times 10^{-4}, 0.1°, 0.1°, -0.1°, -0.1°]^T$
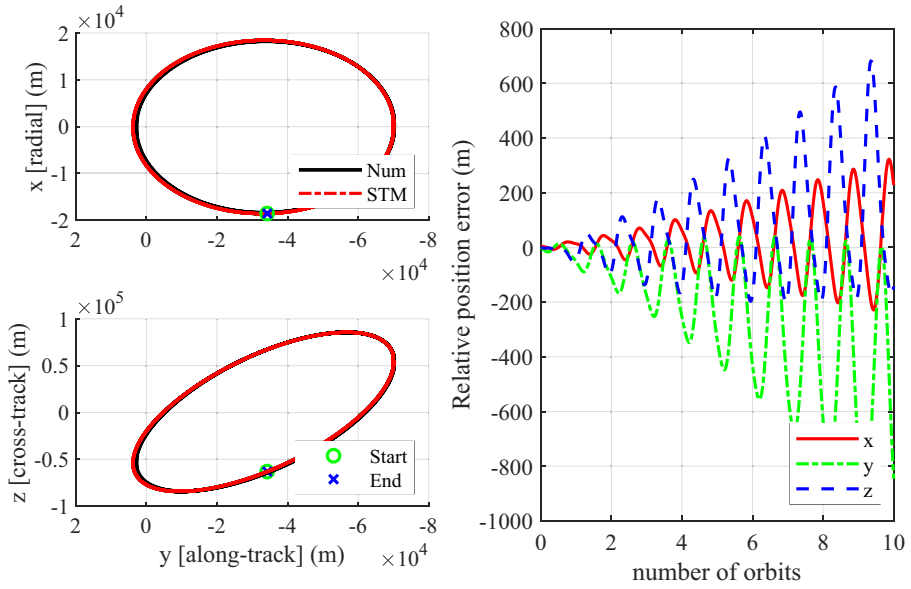
Fig. 8 Proba-3: STM for $e = 0.01$, $\Delta x_0 = [0, 5 \times 10^{-4}, 0.1°, 0.1°, -0.1°, -0.1°]^T$
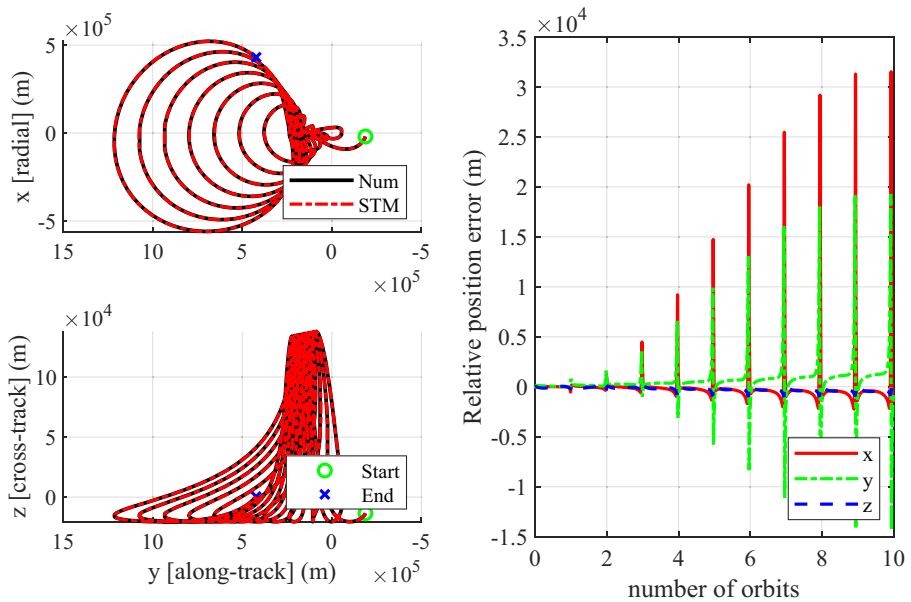
Fig. 9 Proba-3: STM for $i = 90°$, $\Delta x_0 = [0, 5 \times 10^{-4}, 0.1°, 0.1°, -0.1°, -0.1°]^T$
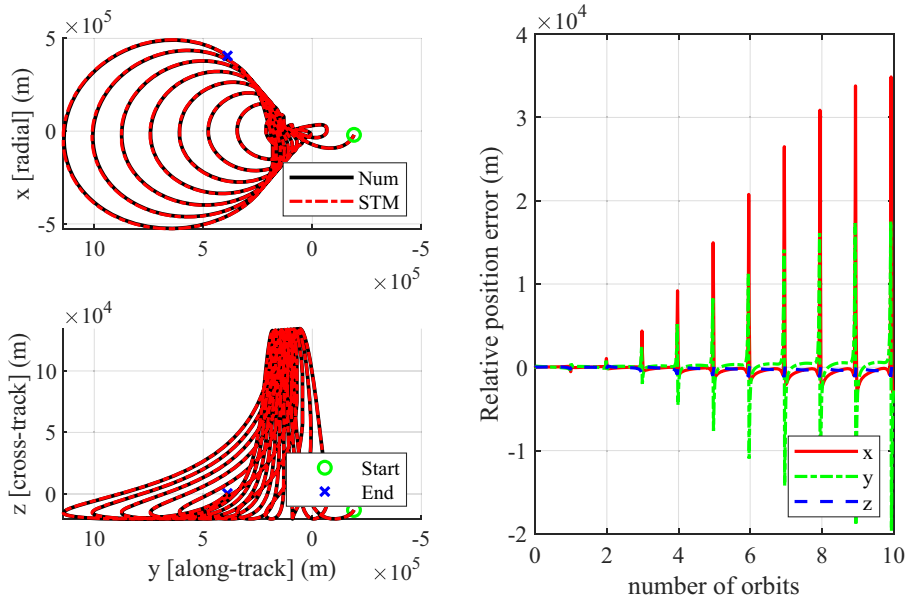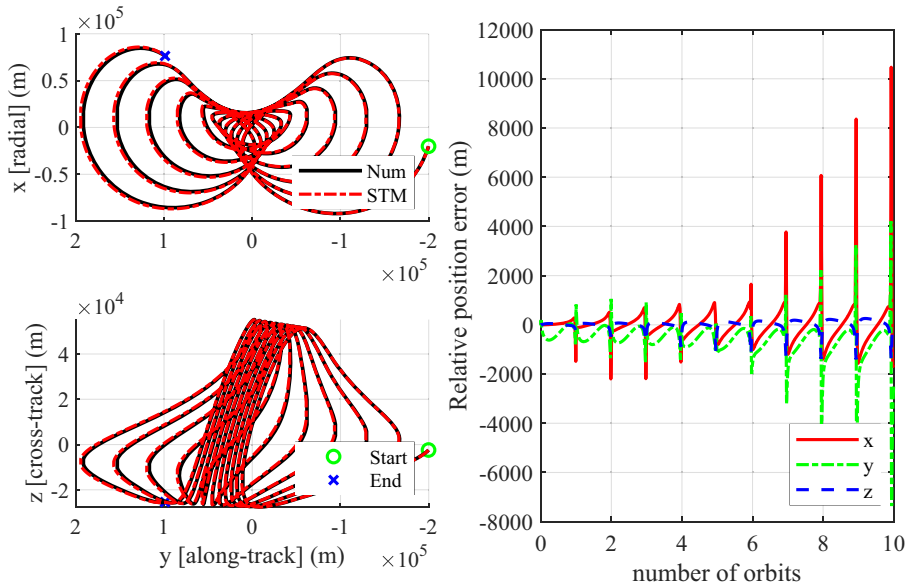
Fig. 10 Proba-3: STM for $i = 75°$, $\Delta x_0 = [0, 5 \times 10^{-4}, 0.1°, 0.1°, -0.1°, -0.1°]^T$

Fig. 11 Proba-3: STM for $i = 40°$, $\Delta x_0 = [0, 5 \times 10^{-4}, 0.1°, 0.1°, -0.1°, -0.1°]^T$
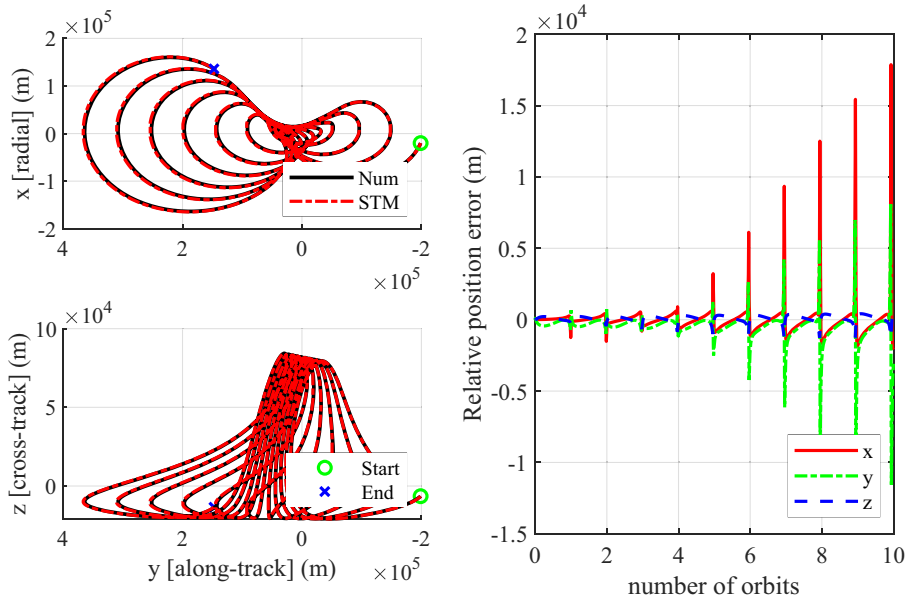
Fig. 12 Proba-3: STM for $i = 25°$, $\Delta x_0 = [0, 5 \times 10^{-4}, 0.1°, 0.1°, -0.1°, -0.1°]^T$


Fig. 13 Proba-3: STM for $i = 5°$, $\Delta x_0 = [0, 5 \times 10^{-4}, 0.1°, 0.1°, -0.1°, -0.1°]^T$

pressure, which is not accounted for in the STM, and third-body perturbations have the highest effect on polar orbits.

The proposed terminal-point guidance law was validated against the same numerical simulator where the sensitivity with respect to time was analyzed by varying the final time from $t_f = 2T$ to $t_f = 15T$ and the obtained results are provided in Figs. 14, 15, 16, 17, 18 and 19. Since the back-propagation is a single-step propagation, this allows to analyze the effects of step-time on the accuracy of the model. In all cases, Alouette-2 was used as the target spacecraft and final desired cartesian coordinates were selected as 2 km in the along-track and radial directions, and no cross-track separation. In all cases, the chaser drifted into the desired position with minimal error when compared to the numerical simulator. However, the main discrepancies were found with the desired back-propagation time, where the calculated initial along track position error increased as the desired time increased. For example, Fig. 17 shows a desired time of 8 orbital periods having desired position errors were less than 100 meters in the along-track direction and no offset in the radial and cross-track directions. On the other hand, Fig. 19 shows a desired time of 15 orbital periods having desired position errors were about 400 meters in the along-track direction and nearly no separation in the radial and cross-track directions. The growth in error are likely caused by the truncation in the Taylor series expansion in the STM formulation.

Table 1 shows the CPU time for each back-propagation case. For each case presented in the table, the CPU time is a collection of ten runs added together within a for-loop to provide the most accurate estimation of computational load. The back-propagation algorithm showed an increase in required computational time as the
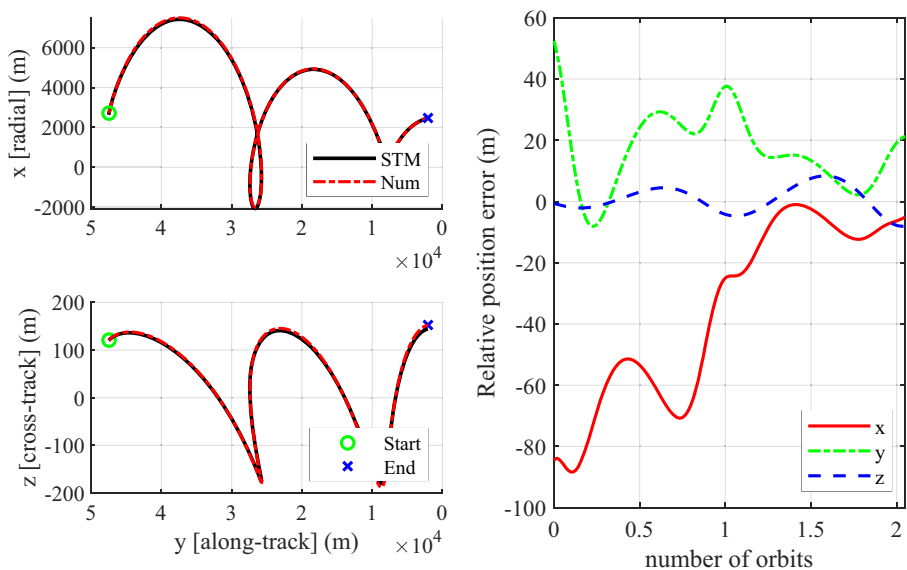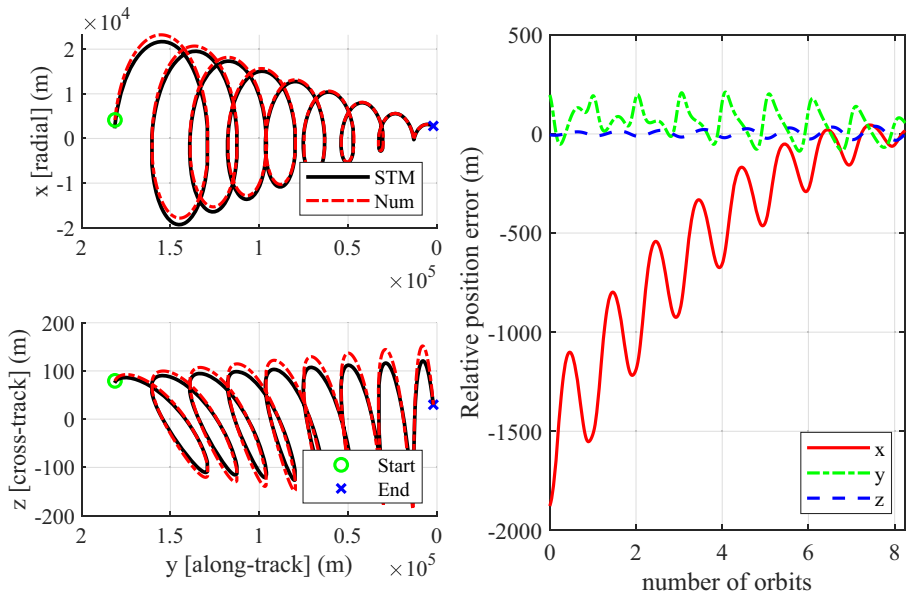

Fig. 14 Alouette-2: Desired Drift Time = 2 Orbital Periods $\Delta x_0 = [2.21\,\text{km}, -9.8086 \times 10^{-6}, 6.37 \times 10^{-6}, -3.71 \times 10^{-2}°, -1.40 \times 10^{-4}°, 0.34°]^T$
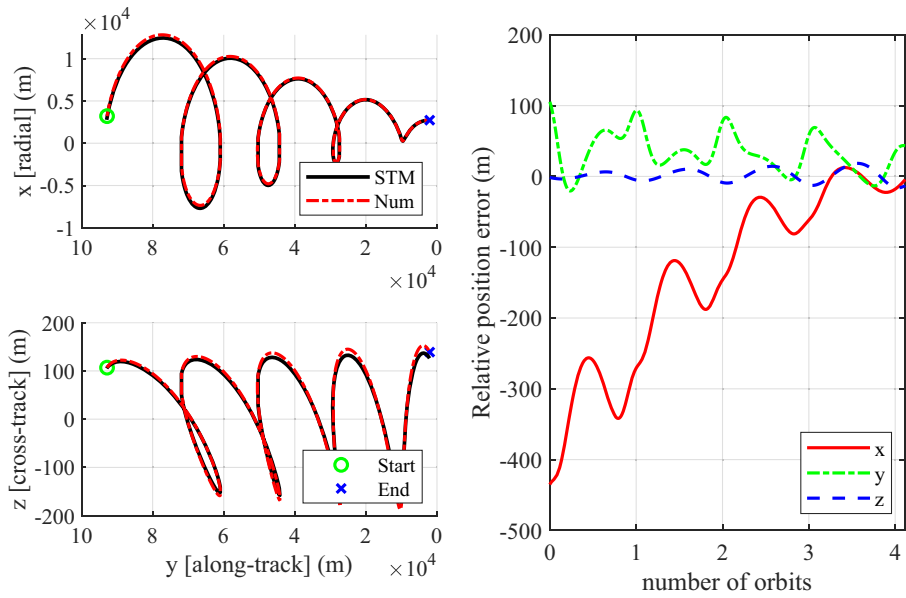
Fig. 15 Alouette-2: Desired Drift Time = 4 Orbital Periods Δx_0 = $[2.21\,\text{km}, -9.0202 \times 10^{-6\circ}, 6.44 \times 10^{-6\circ}, -3.76 \times 10^{-2\circ}, -2.75 \times 10^{-4\circ}, 0.64\circ]^T$
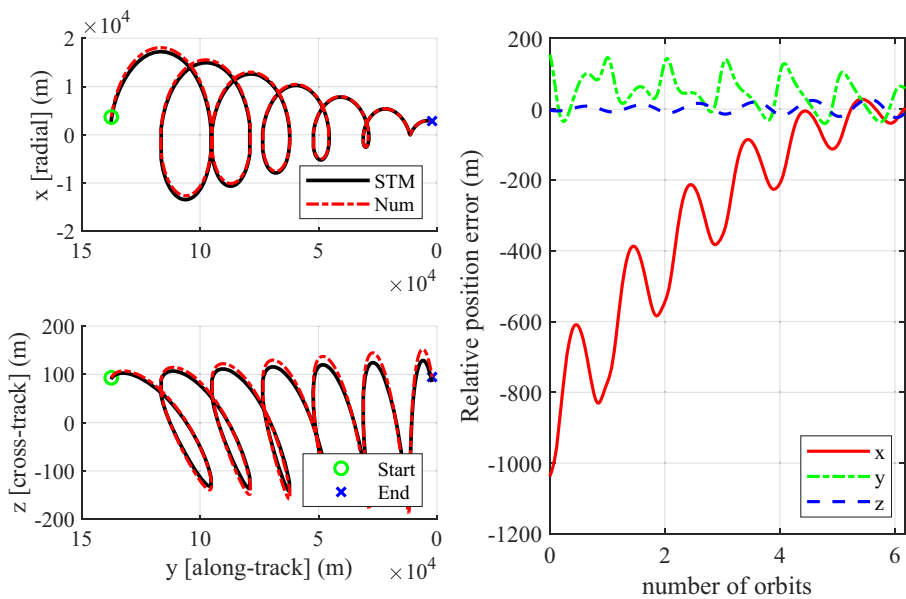
Fig. 16 Alouette-2: Desired Drift Time = 6 Orbital Periods Δx_0 = $[2.20\,\text{km}, -8.2873 \times 10^{-6\circ}, 6.51 \times 10^{-6\circ}, -3.82 \times 10^{-2\circ}, -4.08 \times 10^{-4\circ}, 0.94\circ]^T$
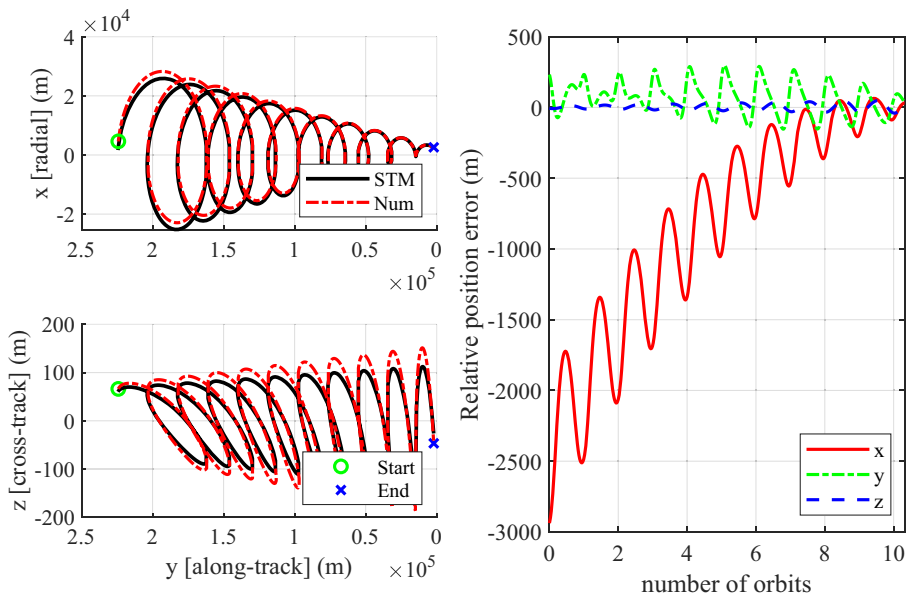
Fig. 17 Alouette-2: Desired Drift Time = 8 Orbital Periods $\Delta x_0 = [2.19\,\text{km}, -7.6086 \times 10^{-6\circ}, 6.58 \times 10^{-6\circ}, -3.87 \times 10^{-2\circ}, -5.41 \times 10^{-4\circ}, 1.23°]^T$

Fig. 18 Alouette-2: Desired Drift Time = 10 Orbital Periods $\Delta x_0 = [2.18\,\text{km}, -6.9827 \times 10^{-6\circ}, 6.64 \times 10^{-6\circ}, -3.92 \times 10^{-2\circ}, -6.72 \times 10^{-4\circ}, 1.52°]^T$
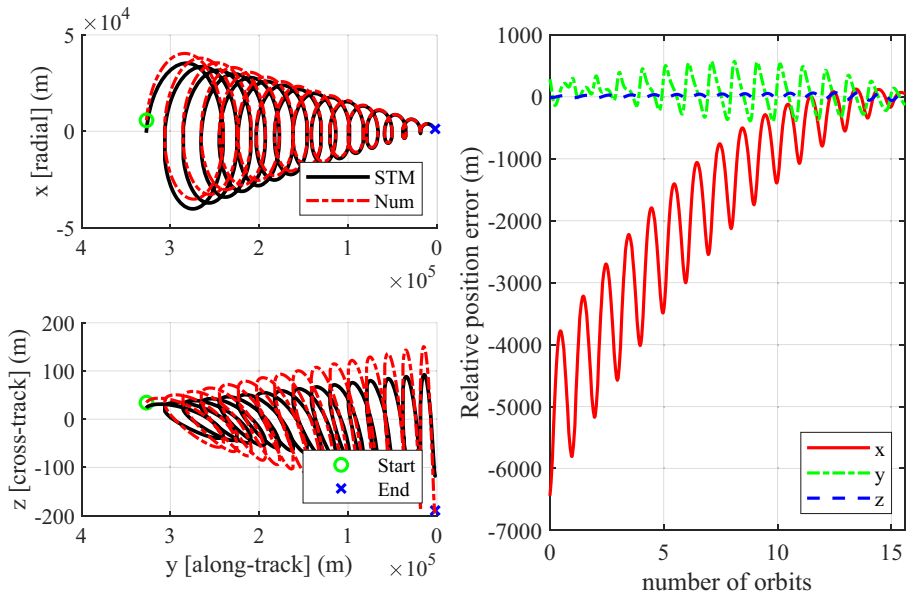
Fig. 19 Alouette-2: Desired Drift Time = 15 Orbital Periods $\Delta x_0 = [2.15\,\text{km}, -5.6394 \times 10^{-6}, 6.76 \times 10^{-6°}, -4.07 \times 10^{-2°}, -9.92 \times 10^{-4°}, 2.23°]^T$

back-propagation duration increase. However, the change is relatively small (on the order of micro-seconds). When comparing the STM computational time to the numerical method, the STM resulted in 4-5 orders of magnitude reduction. Furthermore, as the back-propagation duration increased, the numerical model resulted in a much larger increase in computational time as opposed to the proposed STM. The results are as expected since the STM sacrifices some accuracy for a significant boost in computational efficiency.

Table 1 Computational time (CPU time) in seconds for each back propagation case

Back Propagation Time (Orbital Periods)	STM Formulation CPU Time (sec)	Numerical Propagator CPU Time (sec)
2	0.0061017	16.836537
4	0.0062752	33.679562
6	0.0062299	49.930321
8	0.0064228	76.078415
10	0.0066063	91.589339
15	0.0067833	125.55079

Conclusion

This paper developed a new state transition matrix for spacecraft relative motion under third-body, drag and gravitational perturbations. When the state-transition matrix was compared to the numerical simulator, the solution yielded relatively small errors. Use of the state transition matrix allows for the guidance system to propagate relative motion in terms of relative orbital elements as a linear time-invariant system, since the Jacobian matrices need only be calculated once. In other words, the new solution allows to propagate relative orbital elements by multiplication of constant matrices with time and initial relative orbital elements while considering the effects of J_2 to J_5, fourth order expansion of the third-body perturbation, and atmospheric drag effects on all orbital elements except mean and true anomalies. Previous analysis found in literature addressed the problem of relative motion for long-term analytical propagation; however, the solution presented in this paper was specifically derived for sophisticated guidance and control applications where smaller duration and time-steps are essential in the design. Additionally, the solution presented in this paper does not employ conversion of mean to osculating elements which reduces the computational load while maintaining accuracy. Application of the state transition matrix in the terminal-point guidance law allows for the computation of initial relative orbital elements such that the chaser spacecraft passively drifts into the desired position with a single step. While the solution maintains accurate tracking performance for the terminal-point guidance law, main discrepancies lie within desired time since the state transition matrix is formulated as a Taylor series expansion which needs to be truncated. Future work will be done to include effects of solar radiation pressure within the state transition matrix and apply it two a two-point boundary value problem.

References

1. Appendix, A.: Newton–Raphson Method. Wiley, Hoboken (2003). https://doi.org/10.1002/0471458 546.app1
2. Brouwer, D.: Solution of the problem of artificial satellite theory without drag. Astronom. J. **64**(1274), 378–396 (1959). https://doi.org/10.1086/107958
3. Clohessy, W.H., Wiltshire, R.S.: Terminal guidance system for satellite rendezvous. J. Aeros. Sci. **27**(9), 653–658 (1960). https://doi.org/10.2514/8.8704
4. Cook, G.E.: Luni-solar perturbations of the orbit of an earth satellite. Geophys. J. **6**(3), 271–291 (1962). https://doi.org/10.1111/j.1365-246X.1962.tb00351.x
5. Danielson, D.A.: Semianalytic Satellite Theory. Master's Thesis, Naval Postgraduate School. Monterey, California (1995)
6. Domingos, R.C., deMoraes, R.V., Prado, A.F.B.D.A.: Third-body perturbation in the case of elliptic orbits for the disturbing bodies. Math. Probl. Eng. 2008. https://doi.org/10.1155/2008/763654 (2008)
7. Giacaglia, G.E.O.: Lunar perturbations of artificial satellites of the earth. Celest. Mech. Dyn. Astron. **9**, 239–267 (1972)
8. Gim, D.W., Alfriend, K.T.: State transition matrix of relative motion for the perturbed noncircular reference orbit. J. Guid. Cont. Dynam. **26**(6), 956–971 (2003). https://doi.org/10.2514/2.6924
9. Guffanti, T., D'Amico, S., Lavagna, M.: Long-term analytical propagation of satellite relative motion in perturbed orbits. AAS Spaceflight Mechanics Proceedings 160 (2017)
10. Xu, G., Xu Tianhe, W.C., Yeh, T.K.: Analytic solution of satellite orbit disturbed by atmospheric drag. Mon. Not. R. Astron. Soc. **410**(1), 654–662 (2010)

11. Gurfil, P., Kasdin, N.J.: Nonlinear modeling of spacecraft relative motion in the configuration space. J. Guid. Cont. Dynam. **27**(1), 154–157 (2004). https://doi.org/10.2514/1.9343

12. Gurfil, P., Kholshevnikov, K.V.: Manifolds and metrics in the relative spacecraft motion problem. J. Guid. Cont. Dynam. **29**(4), 1004–1010 (2006). https://doi.org/10.2514/1.15531

13. Gurfil, P., Kholshevnikov, K.V.: Distances on the relative spacecraft motion manifold. AIAA Guidance, Navigation and Control Conference and Exhibit (San Francisco, CA. AIAA paper 2005–5859) (2005)

14. Hamel, J.F., Lafontaine, J.D.: Linearized dynamics of formation flying spacecraft on a j2-perturbed elliptical orbit. J. Guid. Cont. Dynam. **30**(6), 1649–1658 (2007)

15. Hill, G.: Researches in the lunar theory. Am. J. Math. **1**, 5–26 (1878)

16. Inalhan, G., Tillerson, M., How, J.: Relative dynamics and control of spacecraft formations in eccentric orbits. J. Guid. Cont. Dynam. **25**(1), 48–59 (2002). https://doi.org/10.2514/2.4874

17. Izsak, I.G.: Periodic drag perturbations of artificial satellites. Astronom. J. **65**(5), 355–357 (1960)

18. Kaula, W.M.: Development of the lunar and solar disturbing functions for a close satellite. Astronom. J. **67**, 300–303 (1962). https://doi.org/10.1086/108729

19. Koenig, A.W., Guffanti, T., D'Amico, S.: New state transition matrices for spacecraft relative motion in perturbed orbits. J. Guid. Cont. Dynam. **40**(7), 1749–1768 (2017). https://doi.org/10.2514/1.G002409

20. Kozai, Y.: On the effects of the sun and moon upon the motion of a close earth satellite. Smithsonian Astrophysical Observatory (Special Report 22) (1959)

21. Kozai, Y.: The gravitational field of the earth derived from motions of three satellites. Astronom. J. **66**(1). https://doi.org/10.1086/108349 (1961)

22. Kozai, Y.: A new method to compute lunisolar perturbations in satellite motions. Smithsonian Astrophysical Observatory pp. 1–27 (Special Report 349) (1973)

23. Kuiack, B., Ulrich, S.: Nonlinear analytical equations of relative motion on j2-perturbed eccentric orbits. AIAA J. Guid. Cont. Dynam. **41**(11), 2666–2677 (2017). https://doi.org/10.2514/1.G003723

24. Lawden, D.F.: Theory of satellite orbits in an atmosphere. d. g. king-hele. butterworths, london. 1964. 165 pp. diagrams. 30s. J. R. Aeronaut. Soc. **68**(645), 639–640 (1964)

25. Liu, J.J.F.: Satellite motion about an oblate earth. AIAA J. **12**(11), 1511–1516 (1974). https://doi.org/10.2514/3.49537

26. Mahajan, B., Vadali, S.R., Alfriend, K.T.: State-transition matrix for satellite relative motion in the presence of gravitational perturbations. J. Guid. Cont. Dynam. 1–17. https://doi.org/10.2514/1.G004133 (2019)

27. Martinusi, V., Dell'Elce, L., Kerschen, G.: First-order analytic propagation of satellites in the exponential atmosphere of an oblate planet. Celest. Mech. Dyn. Astron. **127**(4), 451–476 (2017)

28. Musen, P., Bailie, A., Upton, E.: Development of the lunar and solar perturbations in the motion of an artificial satellite. NASA-TN D494 (1961)

29. NASA: Spaceflight revolution: The odyssey of project echo (Accessed: January 2019). https://history.nasa.gov/SP-4308/ch6.htm (2019)

30. Prado, A.F.B.A.: Third-body perturbation in orbits around natural satellites. J. Guid. Cont. Dynam. **26**(1), 33–40 (2003). https://doi.org/10.1155/2008/763654

31. Schaub, H.: Incorporating secular drifts into the orbit element difference description of relative orbit. Adv. Astronaut. Sci. **114**, 239–258 (2003)

32. Schaub, H., Junkins, J.L.: Analytical mechanics of space systems. AIAA Amer. Instit. Aeronaut. Astronaut. 593–673 (2018)

33. Sengupta, P., Vadali, S.R., Alfriend, K.T.: Averaged relative motion and applications to formation flight near perturbed orbits. J. Guid. Cont. Dynam. **31**(2), 258–272 (2008). https://doi.org/10.2514/1.30620

34. Smith, D.E.: The perturbation of satellite orbits by extra-terrestrial gravitation. Planet. Space Sci. **9**(10), 659–674 (1962). https://doi.org/10.1016/0032-0633(62)90125-3

35. Roscoe, T.C.W., Vadali, S.R., Alfriend, K.T.: Third-body perturbation effects on satellite formations. J. Astronaut. Sci. **60**(3), 408–433 (2013). https://doi.org/10.1007/s40295-015-0057-x

36. Tooley, C.R., Black, R.K., Robertson, B.P., Stone, J.M., Pope, S.E., Davis, G.T.: The magnetospheric multiscale constellation. Space Sci. Rev. **199**(1), 23–76 (2016). https://doi.org/10.1007/s11214-015-0220-5

37. Vallado, D.A. Fundamentals of astrodynamics and applications, 2nd edn., pp. 80–81. El Segundo, Microcosm Press (2001)

38. Vinti, J.P.: Zonal harmonic perturbations of an accurate reference orbit of an artificial satellite. Math. Math. Phys. 67B(4) (1963)
39. Watson, J.S., Mislretta, G.D., Bonavito, N.L.: An analytic method to account for drag in the vinti satellite theory. Goddard Space Flight Center, Greenbelt, Maryland 71–92 (1974)

Publisher's Note Springer Nature remains neutral with regard to jurisdictional claims in published maps and institutional affiliations.